Hybrid Approaches of Battery Performance Modeling and Prognosis

by

Yangbing Lou

A dissertation submitted in partial fulfillment
of the requirements for the degree of
Doctor of Philosophy
(Mechanical Engineering)
in the University of Michigan
2021

Doctoral Committee

Professor Jun Ni, Chair
Associate Professor Kira Barton
Associate Professor Eunshin Byon
Assistant Professor Jesse Capecelatro

Yangbing Lou

yangbing@umich.edu

ORCID iD: 0000-0001-8806-4719

ACKNOWLEDGEMENTS

First of all, I would like to express my deepest gratitude to my advisor, Professor Jun Ni, for his guidance, care and encouragement through the years. I feel so honored and grateful to pursue my Ph.D. study under his supervision. Without his continuous support and encouragement, this work will not be possible. My sincere thanks also go to my committee members, for their guidance and insights on my research. Special thanks to Dr. Xiaoning Jin, and Dr. Seungchul Lee. My frequent discussions with whom have generated new ideas in my dissertation. I am very grateful for the collaborative environment at the S. M. Wu Manufacturing Research Center. Thanks to George Qiao, Dr. Shuhuai Lan, Kai Chen, Baoyang Jiang, Hao Lei, Xinran Liang, Xun Liu, Xi Gu, Huanyi Shui, and Xin Weng for their help and friendship. Finally, I would like to dedicate this work to my wife, my sons, my parents and parents in law. Their unconditional support and love are the source of my strength. Especially, I would like to thank my wife, Lei, for always believing in me and bringing sunshine into my life.

TABLE OF CONTENTS

LIST OF FIGURES

LIST OF TABLES

ABSTRACT

Batteries, such as Lithium-ion battery, have the advantages of high specific energy, low pollution and high safety, and thus have become one of the main power sources for new energy automobiles. The State of Health (SOH) and Remaining Useful Life (RUL) of a power battery are the most important performance index in the battery system. The SOH of the power battery is different from other battery parameters such as voltage, current, internal resistance and temperature in that it cannot be obtained through direct measurement by any equipment or instrument. Besides, these electrical parameters will degrade with the use of batteries. For this reason, the accurate online estimation of the SOH and RUL of the battery has become one of the key challenges in the battery management system.

This dissertation focuses on investigating key battery performance indicators such as internal resistance, capacity and self-discharge of Ni-H_2 battery and lithium battery. The research also concentrates on the SOH estimation of the batteries through the development of Extended Kalman Filter (EKF) algorithm, the online estimation strategy of Dual Extended Kalman Filter (DEKF) and comprehensive assessment of Particle Filter (PF) and Support Vector Regression (SVR). Data-driven models, such as Autoregressive Moving Average (ARMA) model, artificial neural network, and hybrid models are implemented to provide both the degradation analysis and performance prediction for NiH_2 battery cells. The prediction model can also help reduce the false alarm rate of the existing battery online monitoring system. The long-term behavior of pressure, as a degradation indicator, is modeled to help understand the battery aging behavior.

Combining the electrochemical battery model, a state equation and an output equation for the SOC estimation of the lithium battery are established. Each parameter in the SOC system is observed by using the EKF algorithm. The system simulation results indicate that the SoC estimation of the lithium battery in the EKF algorithm has good precision and accuracy. Furthermore, to solve the problem that the initial parameters of the battery model in the online SOH estimation of the battery cannot be determined in advance, the DEKF algorithm is introduced. Two independent EKFs are established to estimate the state of battery system and the parameters, respectively, and mutually update their states and parameters. The film resistance and discharging capacity are estimated to represent battery's SOH. The advantages of this proposed method are two-fold: (1) implementing physics-based models to provide physical interpretation of Lithium-ion battery cell, and (2) utilizing dual models to maintain the long-term accuracy of estimates.

Finally, a novel battery SOH monitoring model is built to analyze the proposed degradation parameters and to predict the RUL by updating its probability distribution. The Support Vector Regression-Particle Filter (SVR-PF) algorithm is implemented in the research work to make improvement over the standard PF, which has the degeneracy phenomenon. The SVR-PF shows improved estimation and prediction capability compared to the standard PF.

CHAPTER 1

Introduction

1.1 Background and Motivation

With the rapid development in science and technology and the increasing awareness of environmental protection, the new power battery industry has gained a strong momentum of advancement. Power battery refers to the battery with large energy capacity and output power, which can be used in electric bicycles, electric vehicles, electric equipment, energy storage systems, etc. To meet different use characteristics, requirements and application fields, different types of power battery are appropriate: lead-acid battery, nickel-cadmium battery, nickel-hydrogen battery, lithium-ion battery and fuel cell. The factor that power batteries have become a global research hotspot due to the increasing number of private cars and the increasing environmental pollution. Therefore, the development of power batteries and electric vehicles is gaining importance.

The remaining useful life (RUL) of a battery is defined as the effective life left on the battery to meet the performance requirement of operations. The RUL estimation is essential to condition-based maintenance (CBM) and health management. It is important to find a reliable and accurate approach to monitor lithium-ion battery state of health (SOH) and predict the RUL. However, due to the complexity, safety concerns of batteries and various customer usage habits, difficulty arises in accurately estimating the battery energy level, e.g., the state of charge (SOC), monitoring the cell degradation processes, and predicting their remaining useful life.

To estimate the RUL, the first step is to develop a battery model that can reflect the battery's characteristics. The literature of battery modeling is generally categorized into two classes: (1) equivalent circuit models; and (2) physics-based models built upon the knowledge of electrochemical reactions. The equivalent circuit models have limited usefulness for large scale energy applications (e.g., electric vehicles), which require higher accuracy compared to portable electronic applications, especially during operations involving both micro-cycling and deep cycling. In addition, many parameters are required to develop the equivalent circuit model and simulate the complete battery behavior. Furthermore, since the physics parameters are combined as fitting parameters in the equivalent circuit model, the intuition inside a battery is lost. On the other hand, physics-based electrochemical models, including more detailed electrochemical phenomena in modelling, can not only resolve the above-mentioned difficulties, but also improve the estimation and prediction performance of battery cell. Many studies have developed simplified electrochemical-based models that can provide the robust and efficient estimation of battery cell state and parameters without the loss of computational efficiency.

1.2 The State of the Art

1.2.1 Power Battery Model

The equivalent circuit model of a battery does not require the detailed study of the chemical composition and reactions inside the battery. According to the characteristics of battery performance parameters, the equivalent circuit model describing battery system and electrical performance parameters is composed of resistance, capacitance, inductance, power supply and other circuit parameters, which are more concise than that of the electrochemical model.

An important aspect of battery health monitoring and diagnosis is to establish an accurate battery model. The model can simulate the battery behavior and assist in diagnosing the battery problems. The equivalent circuit model is used to calculate the attenuation of battery capacity and obtain the battery health status. However, the equivalent circuit modeling needs to be based on the availability of the large number of experimental data. Each battery life test often takes months or more. There are several types of battery models for the study of battery parameters.

Rint model: Rint model is a simple internal resistance circuit model, which is composed of battery open circuit voltage and internal resistance Rint in series, as shown in Figure 1-1. One of the important indicators of battery health is internal resistance, and the diagnosis method based on the impedance is developing continuously. Coreytl et al. (Coreytl, 2014) proposed a single point impedance method to estimate the SOH of battery pack. This is the simplest basic equivalent circuit model of the battery.

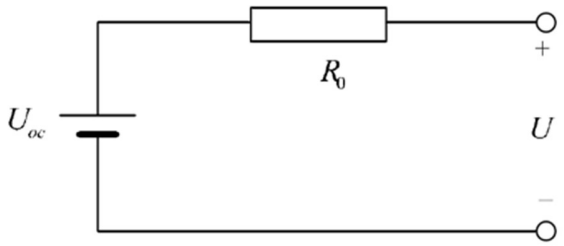

Figure 1-1 Rint equivalent circuit model

Thevenin model: In order to model the complex electrochemical process of a battery, researchers try to use simplified circuit to simulate the performance of the battery. Due to the parallel structure of resistance and capacitance under the action of current, Liaw (Liaw, 2004) and Wang (Wang, 2015) proposed an equivalent circuit to establish battery model to simulate the dynamic and static performance of battery. Hu (Hu, 2012) listed 12 kinds of equivalent circuit models in the literature, and compared and analyzed these lithium battery equivalent circuit models.

In the past 20 years, researchers have established many equivalent circuit models, all of which use voltage, internal resistance and capacity to simulate battery performance. Compared with Rint model, Thevenin model has the advantages of being able to write equations and easily identify the parameters of the model.

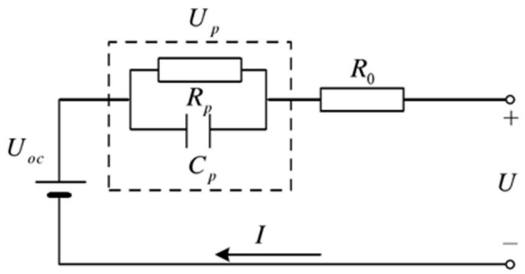

Figure 1-2 Thevenin equivalent circuit model

Combined with the electric equivalent circuit models, the goal of most models is to accurately estimate the state of charge. However, capacity decline, thermal effect and energy density change constantly. Most of the time, the model ignores the influence of these factors on the state of charge. As shown in Figure 1-3, the model includes the runtime model and RC network model, which is similar to the equivalent circuit model. Chen and other scholars (Chen, 2008; Bharath, 2008) proposed that the available capacity of the battery in the model was no longer regarded as a constant, but a function of the number of cycles, battery temperature and storage time. Because the open circuit voltage is a function of SOC, the voltage value can be adjusted according to SOC, but the model is limited in predicting SOH and self-renewal parameters.

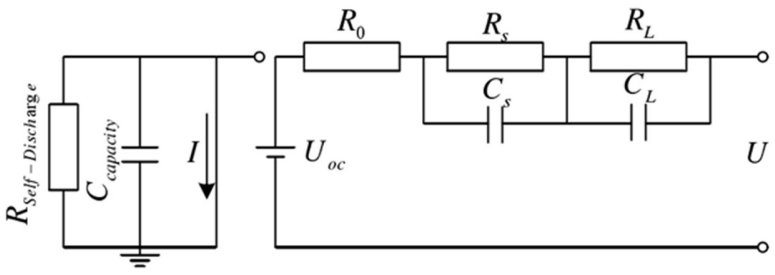

Figure 1-3 Combined with the electronic equivalent circuit model

Electrochemical model: Physics-based electrochemical models include more detailed electrochemical phenomena. The overall chemical reaction for Li-ion battery formula (Smith, 2010)is given by

$$LiCoO_2 + C \leftrightarrow Li_{1-k}CoO_2 + Li_kC \tag{1-1}$$

which can be derived into two electrode reactions.

For positive side, Li^+ ions are extracted from $LiCoO_2$ by oxidation during charging and are inserted into $LiCoO_2$ by reduction during discharging.

$$LiCoO_2 \leftrightarrow Li_{1-k}CoO_2 + kLi^+ + ke^- \tag{1-2}$$

For negative side, Li^+ particles are inserted into Li_kC by reduction during charging and are extracted from Li_kC by oxidation during discharging.

$$kLi^+ + C + ke^- \leftrightarrow Li_kC \tag{1-3}$$

More details of electrochemical models are discussed in Chapter 3.

1.2.2 Battery SOH

The battery SOH refers to the specific characteristics and health status of the used battery compared to the new battery of the same model (Xing, 2011). The battery health degree SOH refers to the ratio of the capacity that the battery can discharge to the rated capacity of the battery under certain conditions. Typically in electric vehicle applications, if the capacity of the battery is less

than 80% of its rated capacity, the user may consider the battery is near the end of life (Meissner, 2005). The SOH of a battery is not only determined by the capacity of the battery, but also by different characteristics of the battery, such as internal resistance and active particle concentrations.

The literature of power battery SOH estimation and prediction mostly focuses on battery capacity degradation and failure mechanism. Kroeze et al. (Kroeze, 2008) and Lee (Lee, 2014) reviewed many popular models and algorithms. The electrochemical behavior of batteries is completely different under different conditions, which brings difficulties to the health monitoring and diagnosis of batteries. First of all, it is difficult to estimate the electrochemical reaction in batteries due to the scarce measurement data obtained by common sensor technology. Secondly, the observable data of battery are normally limited to voltage, current and temperature. Finally, the operating profile of battery is much more dynamic than that of mechanical systems. For example, battery in plug-in hybrid electric vehicles is dominated by driving behavior, electronic equipment and operating environment. Other factors affecting the performance and degradation of batteries include capacity degradation caused by aging, capacity imbalance and self-discharge. Therefore, the uniqueness of power battery system must be considered in the health diagnosis of lithium-ion battery.

Because it is difficult to directly measure the complex electrochemical process inside the battery, most battery health monitoring methods are based on the parameters measured during dynamic operation to understand the chemical reactions inside the battery. Under stable conditions, the battery is placed in a set test program, and the diagnostic model is established by using the measured and collected parameters in the experimental cycles. These parameters include voltage, current, internal resistance and battery temperature, ambient temperature and operating time. This method can avoid the noise interference when collecting data and the influence of battery behavior

uncertainty when charging and discharging. The main disadvantage of this method is that it cannot be implemented online when the battery is in operation.

In most practical applications, an effective and simple way to monitor the battery behavior is to observe the battery voltage, current, temperature and pressure in some cases. These parameters are more suitable for on-line measurement, the measurement process does not need to interrupt the operation of the equipment. Due to the problems of noise, other interference and low quality, online monitoring method can also lead to inaccurate estimation of SOH. Another reason is that the parameter estimation also depends on the accuracy of the sensor. At the same time, the battery management system needs to respond to the output power in milliseconds or even microseconds to avoid the loss of important data. Therefore, the data acquisition system should record the original data with high frequency, otherwise small errors will accumulate with time, which will have a negative impact on the estimation accuracy of battery health.

1.2.3 SOH Estimation and Prediction

Commonly used methods by scholars for SOH prediction of power battery include artificial neural networks, Kalman filters and support vector machine. Starting from the state parameters such as voltage, current, temperature, internal resistance, SOC or capacity of lithium battery, the SOH prediction is realized by the method based on data-driven technology (Li, 2015). Artificial neural networks (ANN) has the characteristics of self-organization and self-learning, which is a nonlinear estimation method in battery SOH estimation algorithm. Artificial neural network is a kind of intelligent network system, which is connected by many interconnected neuron elements. The experimental data of battery life indicates that the battery performance declines with time. Using the rated capacity of the previous cycle to predict the capacity of the next cycle, Ondrej and

other scholars (Ondrej, 2009) trained the input model of voltage and current at three connection times *T*, *T*-1, *T*-2, and ambient temperature. Charkgard et al. (Charkgard, 2009) applied radial basis function to neural network, with the voltage at T-1, SOC and current at t as input.. Mohammad and other scholars (Mohammad, 2010) used the capacity of a single battery as the sample, established the battery capacity estimation model by using the neural network method, and the prediction method had good one-step prediction performance.

Bai, et al. (Bai, 2014) combined adaptive neural network with extended Kalman Filter to estimate the battery SOH, trained the terminal voltage of the battery by adaptive neural network, and then combined with double extended Kalman filter to estimate the SOC and battery capacity. Compared with the equivalent circuit model, the proposed method was more accurate and efficient in SOC and capacity estimation. Han (Han, 2013) proposed to use the fuzzy neural network system modeling, through the influence of various parameters in the battery equivalent circuit model, to estimate the battery health, so as to solve the problem of on-line monitoring of battery deterioration.

Marcol et al. (Marcol,2015) proposed two estimation methods to calculate the SOH of lithium battery. In the first method, according to the capacity decline and battery characteristic curve, and considering the battery operating environment conditions, the fuzzy algorithm was used to calculate the battery health. The second method used neural network to calculate health. Both methods did not rely on electrochemical model, but needed high computing power. The test results showed that both systems had good performance.

1.3 Research Gap and Challenges

Power battery is a complex electrochemical system and the reliable estimation of the SOH and RUL is still of challenge. Its failure mode is affected by many factors, such as the temperature of

the environment, the depth of discharge, the charging and discharging processes and so on. It is very difficult to accurately estimate the health status of the battery by relying on the pure charge and discharge data. The state of health (SOH) of a battery is a measure of battery condition that is affected by time-variant and time-invariant factors. However, most SOH modeling methods only considered time-invariant factors. Besides, researchers commonly rely linearized battery models to implement their developed algorithms, which affects the model accuracy.

1.4 Research Objectives and Framework

The purpose of this research is to develop novel methodologies that can predict the battery's SOH and RUL with high accuracy and robustness. The research will focus on (1) combining physics-based model and data-driven model for the estimation of SOH and RUL of a battery even if the battery has unknown degradation properties, and (2) improving the RUL prediction result even the system and noise have non-linear characteristics. The specific research objectives are summarized as follows:

1. Study the data-driven methods for battery RUL prediction when the battery properties and usage environment are relatively stable.
2. Monitor battery SOH by implementing the dual model structure with unknown degradation related parameters.
3. Develop predictive methodologies to improve the accuracy and robustness of RUL prediction while facing system nonlinearity and noise nonlinearity.

This dissertation is organized as follows. In Chapter 2, a data-driven method is developed to predict the remaining useful life of Ni-H_2 battery. Some physical properties of battery degradation process are considered to improve the prediction accuracy. In Chapter 3, a method is developed to

estimate both the SOC and long-term cell parameters of the battery by integrating a simplified electrochemical battery model and Dual Extended Kalman Filter technique. In Chapter 4, novel battery SOH monitoring models are proposed to analyze the degradation parameters and develop a new approach to predict the RUL by updating its probability distribution. Moreover, the Support Vector Regression-Particle Filter (SVR-PF) algorithm is implemented in the research work to make improvement over the standard PF, which has the degeneracy phenomenon. Chapter 5 provides the conclusion and proposes possible topics for future research work.

A flowchat of the research development and contribution is shown in Figure 1-4 below.

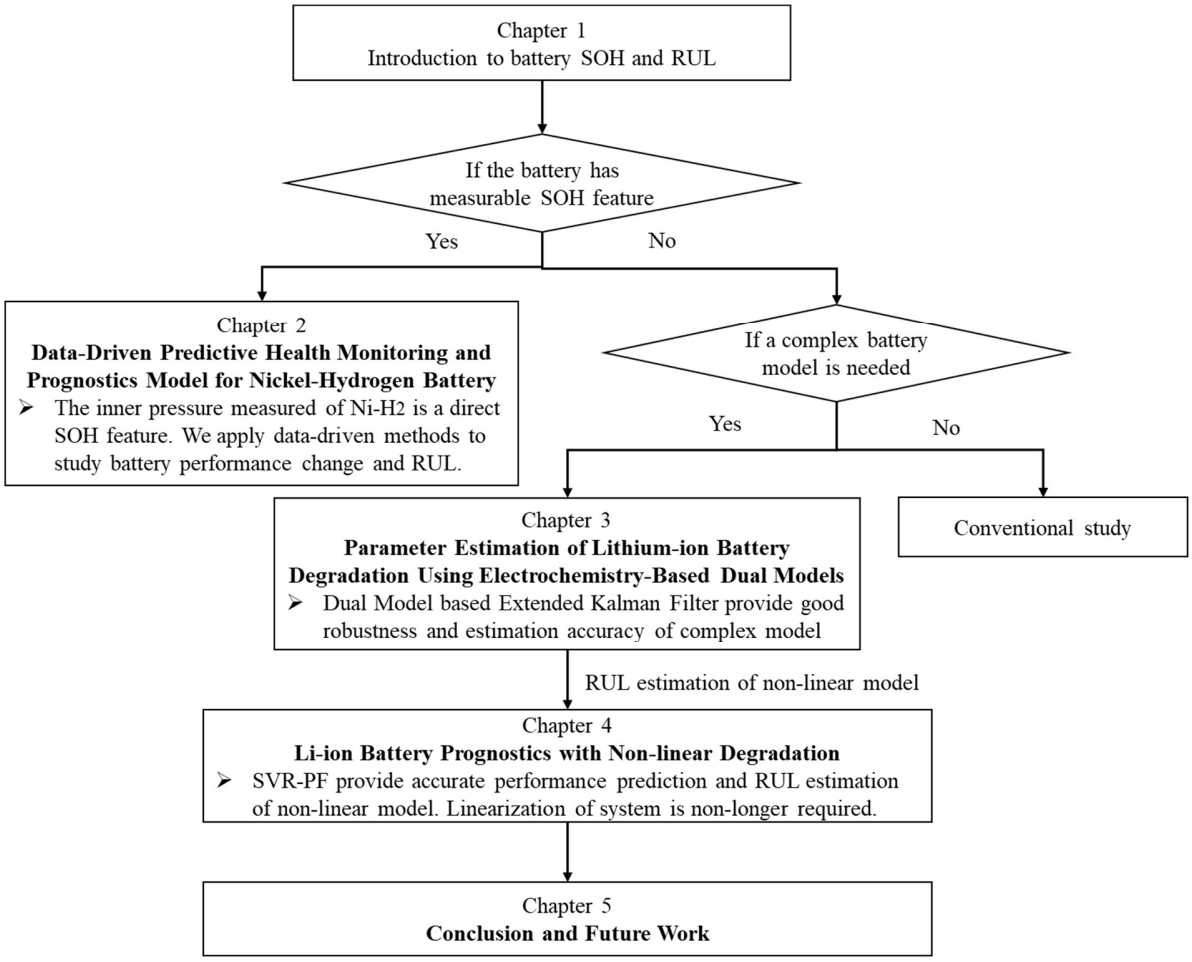

Figure 1-4 Research development and contribution flowchat

CHAPTER 2

Data-Driven Predictive Health Monitoring and Prognostics Model for Nickel-Hydrogen Battery

2.1 Abstract

Nickel-hydrogen (NiH_2) battery plays an important role as an energy storage and support device in applications that require high reliability and long cycle life. The characterization of the battery degradation process with proper health indicator is of importance to the prognostics and health management of the battery system. This chapter investigates data-driven models, such as autoregressive-moving-average (ARMA) model, artificial neural network, and hybrid models to provide both degradation analysis and performance prediction for NiH_2 battery cells using voltage and pressure measurements. The prediction model is designed to reduce the false alarm rate of the existing battery online monitoring system. The accuracy of these methods is compared. The long-term behavior of pressure, as a degradation process indicator, is modeled to help understand the battery aging behavior.

2.2 Introduction

The nickel-hydrogen battery is a rechargeable electrochemical battery that is widely used for its high energy density, excellent overcharge tolerance, long cycle life and high reliability (Smithrick, 1996). The electrochemical reactions during the charging-discharging cycles in the NiH_2 battery are given below.

$$2NiOOH + H_2 \leftrightarrow 2Ni(OH)_2 \tag{2-1}$$

Generally, nickel-hydrogen batteries degrade over time due to aging, environmental impacts, and dynamic loading (Hollandsworth, 2002). Therefore, it is desirable to develop the capability of health monitoring and detection of potential failure risks thus preventing catastrophic failure from occurring in the remote applications such as satellites. In addition to health monitoring and real-time fault detection, it is also valuable to understand how a battery cell degrades and how soon it will reach a performance threshold. To address these two different research issues, various prognostics, and health management (PHM) techniques have been developed in the domain of battery system management (Francisco, 1997).

In recent years, with the emerging development of Lithium-ion battery in automotive and electronics industries, battery State of Charge (SOC) and State of Health (SOH) estimation and health monitoring techniques have garnered significantly increasing attention in the research community. However, the NiH_2 battery has received relatively less attention in the development of health monitoring and prognostics methods.

The characterization of battery performance condition, such as the SOC estimation and health prognostics (RUL prediction) can be generally classified into two categories: data-driven method and physical model-based method. Many approaches of health monitoring and prognostics for Lithium-ion battery cells have been investigated (Goebel, 2008). However, in comparison to

Lithium-ion battery's application domains, NiH_2 batteries are usually used in remote aerospace applications that are inaccessible using sensor technologies resulting in the scarcity of data for analysis. Most available monitoring data collected from NiH_2 battery is discrete-time values such as voltage, current, temperature and pressure. Other challenging issue for the performance degradation analysis is the limited understanding of the long-term cycling-based aging effects such as capacity loss, self-discharge, etc. Therefore, the uniqueness of the NiH_2 battery system and limited data availability need to be considered for the development of appropriate methodologies for NiH_2 battery health monitoring and prognostics.

To precisely monitor and predict battery's performance and health, it is essential to determine the appropriate performance indicators to characterize the health condition of the battery cells. In a battery system, voltage is usually one of the widely used observable states and indicator of a battery current performance. A typical NiH_2 battery voltage varies from 1.5V to 1.25V, when it is discharged from full capacity to nearly empty capacity (Zimmerman, 2008; Zhang, 2011). The voltage change of one discharge-charge cycle is shown in Figure 2-1. It is necessary to track the cell voltage behavior to detect any abnormal conditions and even failures during its operation life. If battery follows a predetermined working load, its voltage change during the long run can be predicted and the predicted value can be further used as a reference to detect abnormal condition.

Besides voltage, the battery inner pressure is also a very robust battery performance indicator. The chemical reaction in Eqs. (2-1 and 2-2) shows that the produced oxygen and hydrogen gas will result in proportional relationship between cell pressure and remaining capacity (Zimmerman, 2008). In other words, a maximum pressure during a discharge-charge cycle can present the end-of-charge cell pressure, which is also the maximum pressure during a cycle. A mean value of the pressures in a discharge-charge cycle can reflect the discharged capacity. Hence, we can use the

maximum pressure and mean pressure to reflect a cell's health and performance from different perspectives. Considering the complication of the degradation mechanism of the NiH_2 battery, we need to investigate both to analyze the degradation process.

Comparing to the end-of-charge voltage (Francisco, 1997), charging and discharging efficiency (Zimmerman, 2008), and other features, it is known that the vessel pressure growth in nickel-hydrogen cells is one of the most direct degradation indicators. The nickel sinter in the nickel electrodes will generate hydrogen gas due to its corrosion during the whole battery life cycle. Besides, the pressure increases as well as other corrosion related degradation process, always involve a nearly linear increment during battery's life cycle. Based on loading condition and manufacturing variation, the pressure growth rates, and growth pattern can vary significantly from cell to cell. Figure 2-2 shows a pressure growth pattern of a typical Independent Pressure Vessel (IPS) nickel-hydrogen cell. In this chapter, we focus on the pressure growth for the prognostics of a single cell, not the growth variation among different units.

Though pressure is a meaningful indicator, special attention needs to be paid since in most experiment, strain gauges are attached to the cells to measure cell pressure, and during the long run the strain gauge may drift (Zimmerman, 2008). Without correct gauge installation and drifts analysis, such cell pressure indications can be used for information only. To indicate the correct pressure of cell, the bonding condition between gauge and cell should be properly verified and controlled to avoid rapid drift. Such measurements have been taken for some nickel-hydrogen cells after long-term life testing and it is not unusual to find a 100-200 psi drift in the strain gauge pressure reading after 10 or more years of cell operation. However, in our experiment, we have verified the measurement and collected the correct data.

Self-discharge (SD) rate is another important indicator of NiH_2 battery performance

(Purushothaman, 2012). A typical vessel may suffer 5-10% capacity loss per month if the battery is placed above 0℃ in an open circuit state (Iwakura, 1989). The SD process is an interesting phenomenon to be investigated and studied. There are research works done to build the SD physical model (Purushothaman, 2012) to determine the SD rate at any time and temperature.

In this chapter, we develop data-driven methods using available past time series data for two different purposes: (1) real-time fault detection; and (2) the prognostic prediction of long term cell performance using time series data.

2.3 NiH_2 Experiment Description

NiH_2 battery is widely used in aerospace and this experiment simulates a low earth orbit (LEO) environment and corresponding workload for NiH_2 battery life testing. The temperature will be kept between -10℃ and 0℃. A similar repeated one-day working pattern was implemented on a battery pack of 27 identical Independent Pressure Vessels (IPV) connected in series.

The total experiment had been run for 3.5 years and each one year was divided into 5 segments: idle time, operating season 1, idle time, operating season 2, and idle time. Every year, there were two battery operation seasons and during the season the battery was charged and discharged once per day for about 44 days. The discharging proceeded within 2 to 5 hours to simulate the operation situation when a satellite was in the earth shade. The depth of discharge varied from 10% to 80%, which increased the derogation process (Iwakura, 1989). After discharging, the battery was charged back to its full capacity by 4A constant current, while the end-of-charge process was terminated by a voltage trigger when voltage reached 41V. Thereafter during the idle time, the battery was charged by a 0.4A current to compensate for the self-discharge effect. The demonstration of 1 day measurements [current (I), voltage (V), pressure (P), and temperature (T)],

and pressure of 352 battery operating days is shown in Figure 2-1.

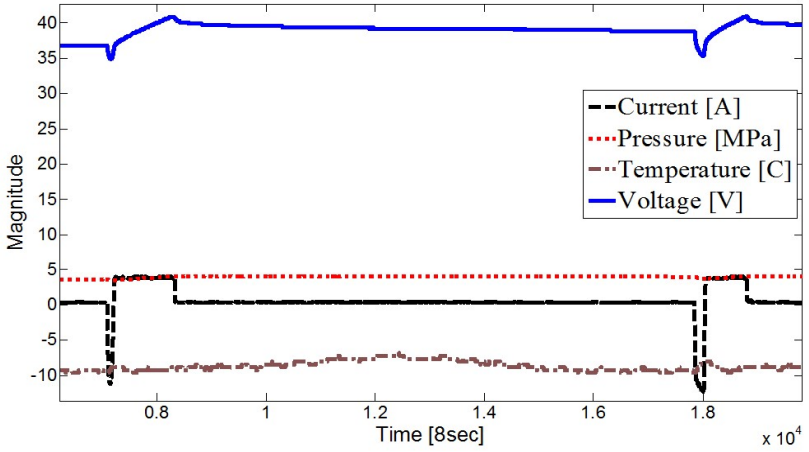

Figure 2-1 NiH_2 battery one day measurements: current (I), voltage (V), pressure (P), and temperature (T)

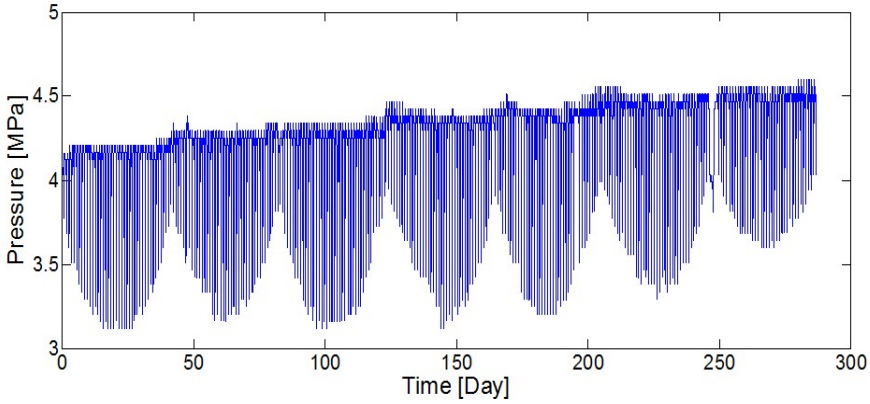

Figure 2-2 NiH_2 battery pressure measurements in time series

2.4 Description of Methodologies

2.4.1 Autoregressive Moving Average Model (ARMA) for time series analysis

Time series analysis and prediction based on stochastic process theory and mathematical

statistics have been widely applied in signal processing, intelligent information analysis and PHM. Among these tools, autoregressive moving average (ARMA) model is a widely used tool for understanding data properties and predicting future values of this time series. The ARMA model aims to explain data by using time series data on its past values and uses linear regression to make predictions.

The "AR" in ARMA stands for autoregression, indicating that the model uses the dependent relationship between current data and its past values. In other words, it shows that the data is regressed on its past values. Stationarity is assumed for time-series data, which is made "stationary" by subtracting the observations from the previous values.

The "MA" stands for moving average model, indicating that the forecast or outcome of the model depends linearly on the past values. Also, it means that the errors in forecasting are linear functions of past errors. Note that the moving average models are different from statistical moving averages.

$$ARMA(p,d,q) \times (P,D,Q):$$

$$\Phi(B^h)\phi(B)\nabla_h^D \nabla^d y_t = \alpha + \Theta(B^h)\theta(B)\varepsilon_t \tag{2-2}$$

The coefficients of autoregressive terms are:

Non-seasonal Part: $\phi(B) = 1 - \phi_1 B - \cdots - \phi_p B^p$

Seasonal Part: $\Phi(B^h) = 1 - \Phi_1 B^h - \cdots - \Phi_P B^{Ph}$

The coefficients of moving average consist of two parts:

Non-seasonal Part: $\theta(B) = 1 + \theta_1 B + \cdots + \theta_q B^q$

Seasonal Part: $\Theta(B^h) = 1 + \Theta_1 B^h + \cdots + \Theta_P B^{Ph}$

where y_t is the time series data to be predicted, B is the lag operator, which is defined as $By_t = y_{t-1}$, ∇ is the difference operator, which is defined as (1 - B). Besides, p is the number of autoregressive (AR) terms, d is the differencing order of non-seasonal series, and q is the number of moving average (MA) terms. For the seasonal part, P is the number of seasonal autoregressive (SAR) terms, D is the number of seasonal differences, Q is the number of seasonal moving average (SMA) terms, h is the length of the seasonal period. $\alpha = \eta(1 - \phi_1 - \cdots - \phi_p)$ and $\phi = E(\nabla^d y_t)$, which is the expected value of the differenced data. A detailed seasonal ARMA model establishing procedure can be found in (Box, 1976).

2.4.2 Artificial neural networks (ANN)

ANN, which consists of various nodes and layers, is a simple imitation of human brain. It requires little expert knowledge in modeling complex systems and adopts a “black box” approach to various sources of data. Due to its simplicity in handling data in complex or even unknown systems, ANN has become one of the most widely used methods in complex system modeling. A typical neural network consists of 3 layers: an input layer, a hidden layer, and an output layer. Depending on the specific needs, such as the number of inputs and outputs, the number of nodes within different layers can be defined. The lines linking each pair of nodes are denoted as weights, which are mapping functions from one space to another. (Hassoun, 1995)

2.4.3 ARMA+ANN Hybrid model for one step prediction and fault detection

Traditionally, ARMA model is used as a linear stationary model for time series analysis and prediction. In practice, however, many time series include both linear and nonlinear autocorrelation properties. Therefore, it is useful to use a combined structure of both linear and

nonlinear models to deal with this signal.

A hybrid nonlinear time series predictor consists of an ARMA based linear predictor and a nonlinear predictor using Artificial Neural Network (ANN). The design of this hybrid predictor is simply inspired by the existing hybrid neural predictors developed for nonlinear time series prediction (Dalton, 2004; Haykin, 1995).

The ARMA model, as a linear sub-predictor, provides a base model for the time series. The residuals from the model are then fed into a nonlinear one-layer recurrent neural network, which is used as a nonlinear sub-predictor. Such integration of linear and nonlinear prediction is built as a hybrid model:

$$y_t = L_t + N_t \tag{2-3}$$

where L_t is linear component obtained in an ARMA and N_t is the residual that can be estimated from an ANN model.

The hybrid model consists of three main steps:

Step 1. Develop the base model by using ARMA, obtain the linear component $\widehat{L}_t$, and then compute the residuals:

$$e_t = y_t - \hat{L}_t \tag{2-4}$$

Step 2. Establish the ANN model by using residuals e_t:

$$\widehat{N}_t = e_t = b_0 + \sum_{j=1}^{q} w_j g\left(b_{0j} + \sum_{i=1}^{p} w_{ij} e_{t-i}\right) + \varepsilon_t \tag{2-5}$$

Step 3. Add $\hat{L}_t$ and $\widehat{N}_t$ to conduct time series prediction:

$$\hat{y}_t = \hat{L}_t + \widehat{N}_t \tag{2-6}$$

We use the hybrid model for one-step-ahead prediction and abnormal data detection.

2.5 Health Indication and Prediction

2.5.1 One-step ahead prediction and anomaly detection

We apply three methods to perform one-step-ahead prediction, which is used for an online anomaly detection process. The hybrid model provides the confidence interval of the data, so we develop an online approach to detect the abnormal condition of cell. First, the cell data is predicted one step ahead using the hybrid model, and the confidence interval is also calculated. Second, a new measurement is compared to the predicted confidence interval. If the new measurement is beyond this boundary, an abnormal point is detected.

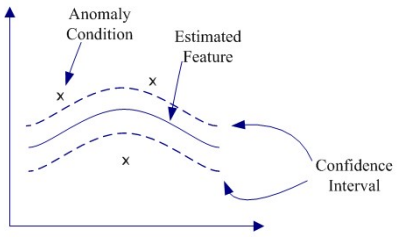

Figure 2-3 Illustration of anomaly detection

We have the experiment data in normal condition, and the false alarm rate is type I error. The false alarm rates and the performance of one-step-ahead prediction by calculating the Mean Squared Error (MSE) among the ARMA, ANN and hybrid models are shown in Figures 2-4, 5 and 6. There are two subplots in each figure, the upper subplot shows the general prediction results of each model, and the lower subplot represents the zoomed in area of the specific region of the general results.

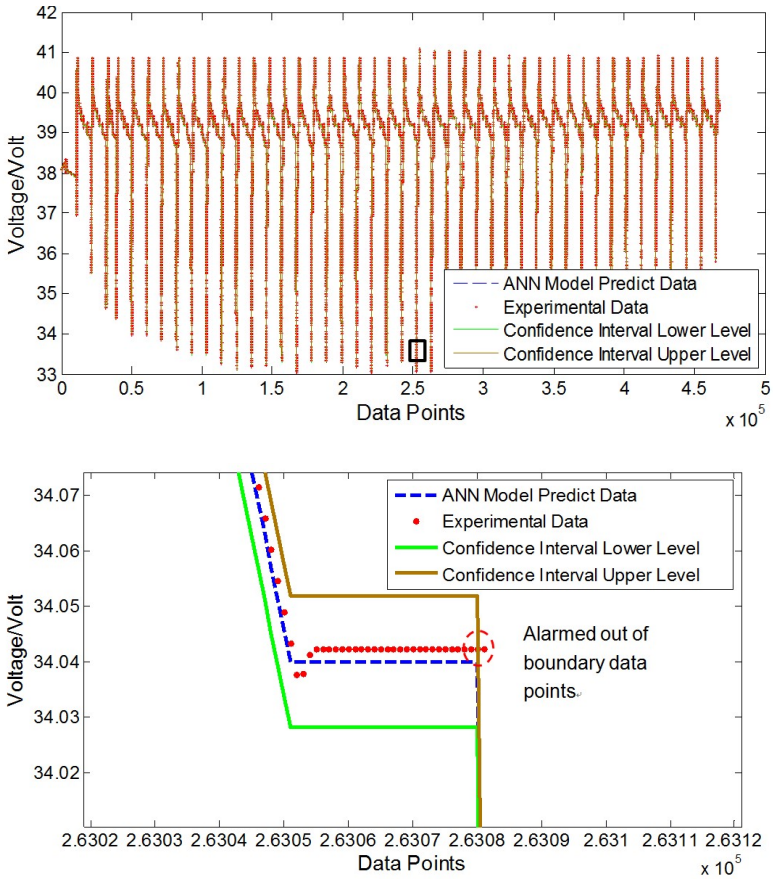

Figure 2-4 Data in red locate outside the confidence interval of ANN model prediction

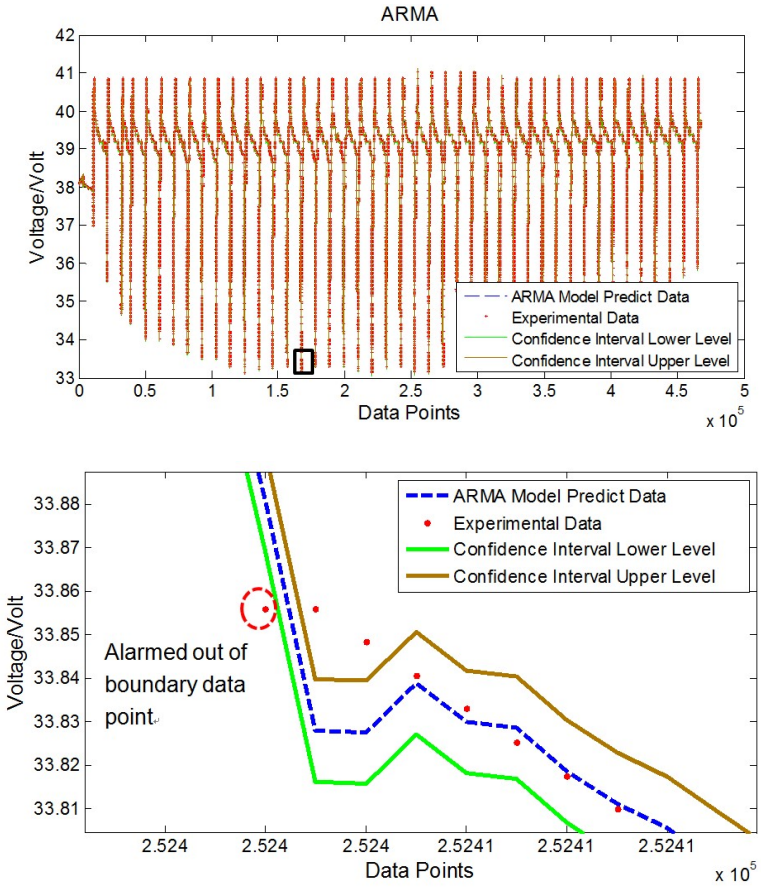

Figure 2-5 Data in red locate outside the confidence interval of ARMA model

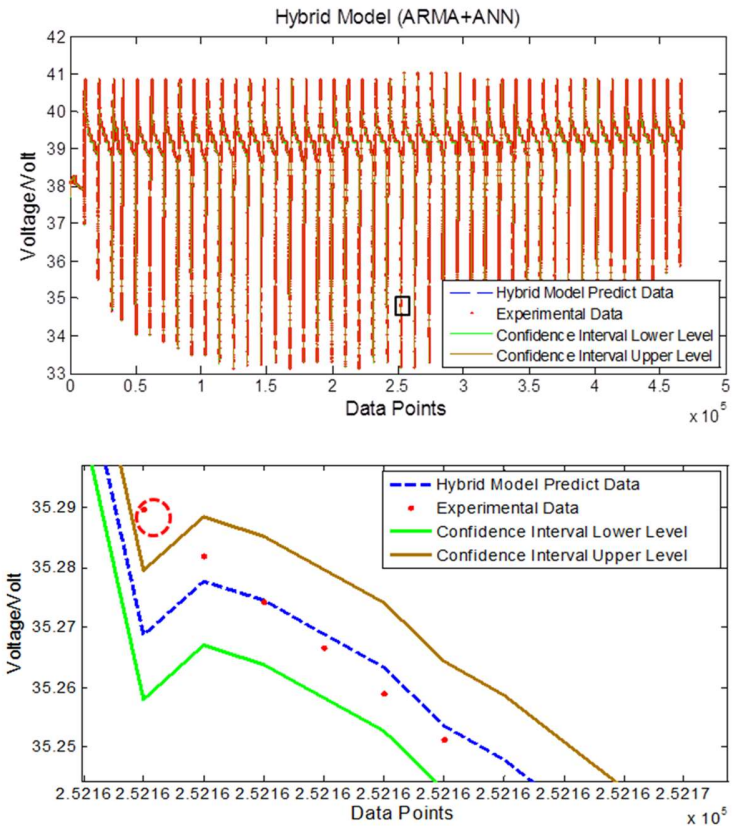

Figure 2-6 Data in red locate outside the confidence interval of hybrid model

We compare the performance of all three models in terms of the false alarm rate and the mean squared error (MSE) of the one-step-ahead prediction, as shown in Table 2-1. The result shows that the hybrid model provides significantly lower false alarm rate than the standard ANN model and standard ARMA prediction approach (by 40.57% and 66.47% improvement, respectively). In addition, the hybrid model provides the most accurate one-step-ahead prediction among the three methods with the lowest MSE value. The improvements are 36.97% and 49.45% compared with ANN model and ARMA model, respectively.

Table 2-1 Summary of accuracy and false alarm rate

	ANN	ARMA	Hybrid
False Alarm Rate	2.81%	4.98%	1.67%
MSE	0.0660	0.0823	0.0416

2.5.2 Long term pressure prediction

As described in the introduction section, the pressure growth in nickel-hydrogen cells is the normal phenomenon of degradation process. We use the end-of-charge pressure in each charging-discharging cycle for the pressure growth analysis. The end-of-charge is controlled by a voltage trigger such that the charging process is stopped when the voltage reaches 41V. During the battery life span, the capacity gradually fades, and less electricity can be charged into the battery. It can be assumed that if there is no pressure growth due to extra hydrogen generated, the end-of-charge pressure should decrease. However, from Figure 2-7, we can see that the maximum pressure (equivalent to the end-of-charge pressure of each working day) increases gradually. Besides, the pressure degradation also occurs during the idle time, but it is not of our interest since it is charged by a 0.4A current and during the whole period the battery will not be charged back to its full capacity. The pressure will not reach its maximum and hence the measurement cannot directly reflect its degradation.

Besides the end-of-charge pressure, the mean pressure is also used for pressure growth analysis because it indicates the daily working load or discharged capacity. The lower mean pressure of one day means the more electricity the battery has consumed. Ideally, the pressure should remain the same if there is no battery degradation and capacity fade. Figure 2-7 shows the mean pressure throughout the 7 seasons increases gradually. The red point indicates the start of each season.

In literature, it is mentioned that the strain gauge may drift during long term. However, the experiment lasts only about 400 cycles in 3.5 years and we setup and controlled the gauge properly. Hence, the gauge drifts can be ignored in this study. The mean pressure and the maximum pressure are used as the degradation indicator for battery degradation prognostics.

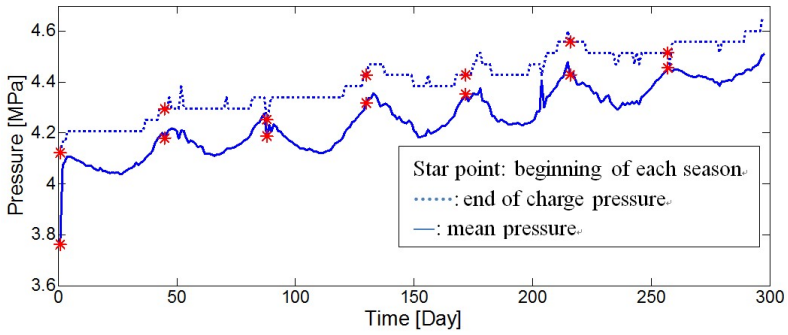

Figure 2-7 Pressure long term behavior and its maximum and mean pressure

To investigate the pressure variation, a data driven model, ARMA with seasonality is developed. The model is built based upon both the maximum pressure data and the mean pressure data, with notation shown below:

$$ARMA(p,d,q)\times(P,D,Q):$$

$$\Phi(B^h)\phi(B)\nabla_h^D\nabla^d y_t = \alpha + \Theta(B^h)\theta(B)\varepsilon_t \tag{2-8}$$

The coefficients of autoregressive terms are:

Non-seasonal Part: $\phi(B) = 1 - \phi_1 B - \cdots - \phi_p B^p$

Seasonal Part: $\Phi(B^h) = 1 - \Phi_1 B^h - \cdots - \Phi_P B^{Ph}$

The coefficients of moving average consist of two parts:

Non-seasonal Part: $\theta(B) = 1 + \theta_1 B + \cdots + \theta_q B^q$

Seasonal Part: $\Theta(B^h) = 1 + \Theta_1 B^h + \cdots + \Theta_P B^{Ph}$

where y_t is the time series data of pressure, B is the lag operator, which is defined as $By_t = y_{t-1}$, ∇ is the difference operator, which is defined as (1 - B). Besides, p is the number of autoregressive (AR) terms, d is the differencing order of non-seasonal series, and q is the number of moving average (MA) terms. For the seasonal part, P is the number of seasonal autoregressive (SAR) terms, D is the number of seasonal differences, Q is the number of seasonal moving average (SMA) terms, h is the length of the seasonal period. $\alpha = \eta(1 - \phi_1 - \cdots - \phi_p)$ and $\phi = E(\nabla^d y_t)$, which is the expected value of the differenced data. A detailed seasonal ARMA model establishing procedure can be found in (Box, 1976).

With the inspection of sample Autocorrelation Function (ACF) of original data and sample ACF of first differenced data in Figure 2-8, the orders of the model $(p,d,q)\times (P,D,Q)$ are initialized. We assume that the conditional probability distribution is Gaussian.

The ARMA model is trained by the method of least squares. The Akaike information criterion (AIC) (Akaike, 1974) was used to investigate the model complexity while the t-statistics was used to investigate the significance of model parameters. The refined model trained by 300-day data is concluded in Table 2-2. The coefficients of AR(4) and MA(1) have the most impact on the system behavior. The insignificant coefficients have been removed from the model.

The model also gives the minimum AIC, which is -1.532E03. Besides, the seasonality is waived since it increases the model complexity while the accuracy is not improved significantly. The false alarm rate calculated by Eq. 2-7 is based on the 95% confidence interval (CI) and mean square error (MSE), which is determined as:

$$CI = Y_t \pm 1.96\sqrt{MSE} \tag{2-9}$$

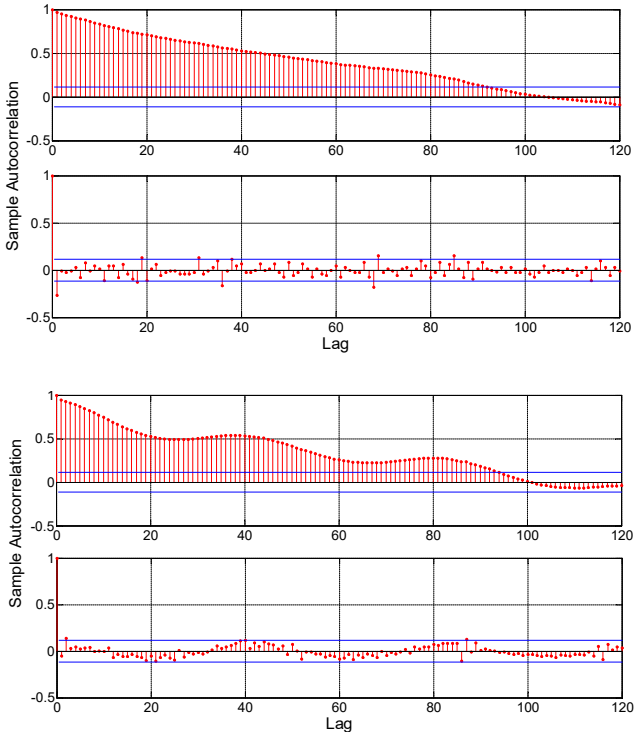

Figure 2-8 Sample ACF of maximum (upper) and mean pressure (lower) and their first difference

Table 2-2. Maximum pressure model: ARIMA(4,1,5)

Parameter	Value	Error	t Statistic
Constant	3.36E-03	1.55E-03	2.16
AR{2}	-6.20E-01	1.61E-01	-3.86
AR{4}	-5.75E-01	9.39E-02	-6.12
MA{1}	-3.21E-01	4.40E-02	-7.30
MA{2}	6.46E-01	1.63E-01	3.97
MA{3}	-2.60E-01	7.27E-02	-3.58
MA{4}	6.38E-01	9.83E-02	6.49
MA{5}	-3.31E-01	4.96E-02	-6.67
Variance	3.24E-04	1.60E-05	20.27

After training the model from the data of first 250 days, we predict the maximum pressure over the next 50 days by implementing *multi-step* prediction techniques. The corresponding

confidence interval is also calculated. We also predict the next 90 days maximum pressure value using 200 days measurements as training data. The results are shown in Figures 2-9 and 2-10. Both test results validate the accuracy and robust of our data driven model.

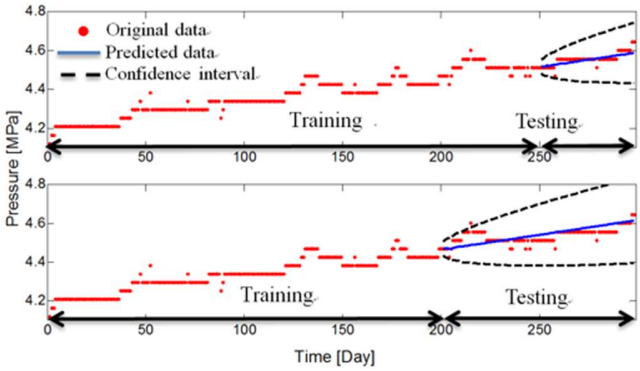

Figure 2-9 Upper: 50 days ahead maximum pressure prediction; Lower: 90 days ahead maximum pressure prediction

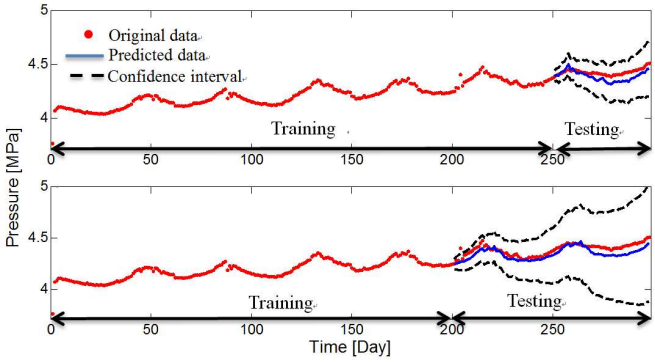

Figure 2-10 Upper: 50 days ahead mean pressure prediction;
Lower: 90 days ahead mean pressure prediction

Both the maximum pressure and the mean pressure show the battery degradation process of to pressure growth. The maximum pressure increased by 9.5% and the mean pressure increased by 12.5% for 3.5 years. We forecast the following 150 working days, which is about 1.5 years pressure performance by adapting the ARMA model. The model structure is the same as in Table 2-2.The

prediction results are shown in Figure 2-10. It is expected to see that the maximum pressure will increase to 5.07MPa and the mean pressure will increase to 4.74MPa. If the tolerated pressure is known, the RUL can be estimated based on our prediction. The confidence interval increases rapidly but can be used as early-warning of the failure caused by pressure growth.

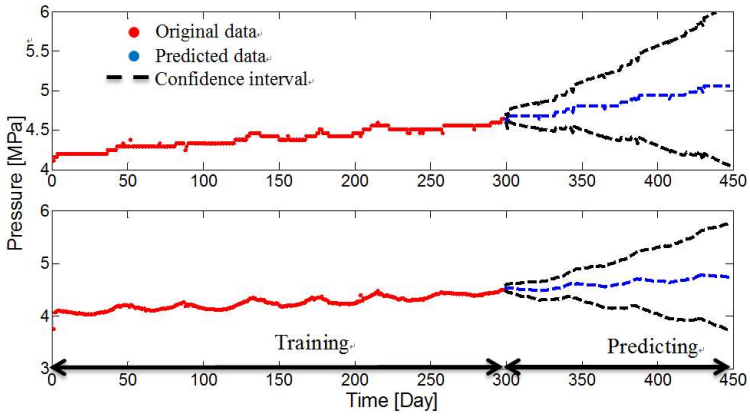

Figure 2-11 150 working days pressure prediction; maximum pressure (upper); mean pressure (lower)

In addition to long term prediction, we implement one-step-ahead prediction for both mean and maximum pressures to examine the pressure variation of everyday. The confidence interval is constructed based on the corresponding degree of freedom to help detect abnormal point and reduce the false alarm rate. The results are shown in Figure 2-12 and Figure 2-13.

Most abnormal points detected are at where there is a sudden change of either the original time series or confidence interval. The false alarm rate for maximum pressure is 11.0% (32/291) while the false alarm rate for mean pressure is 0.83% (2/240).

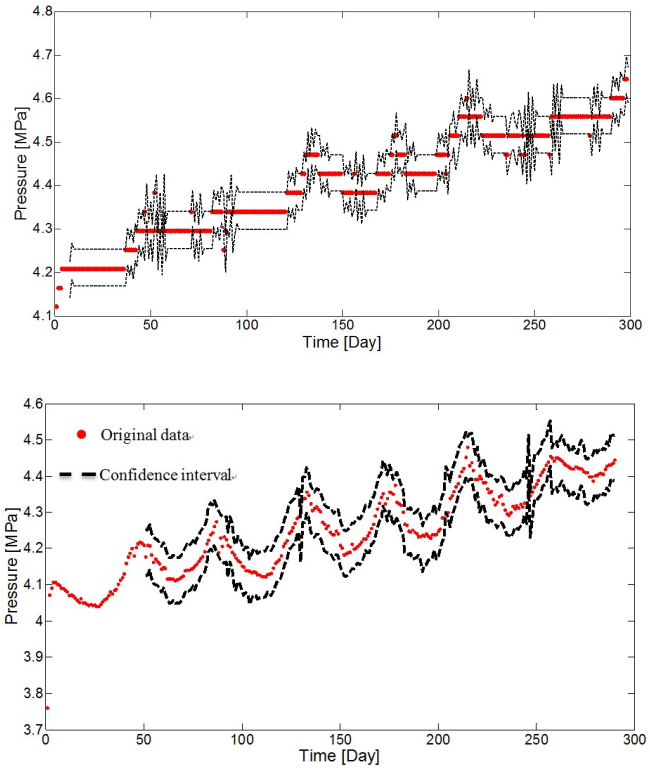

Figure 2-12 One-step ahead prediction for maximum pressure (upper) and mean pressure (lower)

Most of the abnormal points monitored are related to the measurement of the maximum pressure. The end-of charge trigger might not work properly during the experiment and sometimes the battery was overcharged, which incurred the maximum pressure variation. Although those points of maximum pressure alarmed are false alarm, it still provides valuable information about pressure variation, and gives decision support of how to select the end-of-charge trigger to avoid large battery overcharge. Furthermore, if we combine both the mean and the maximum pressure, it can be concluded that there is no point lying outside both confidence intervals. Hence, the maximum and mean pressure can help reduce the false alarm rate to zero and give better result than using only one feature.

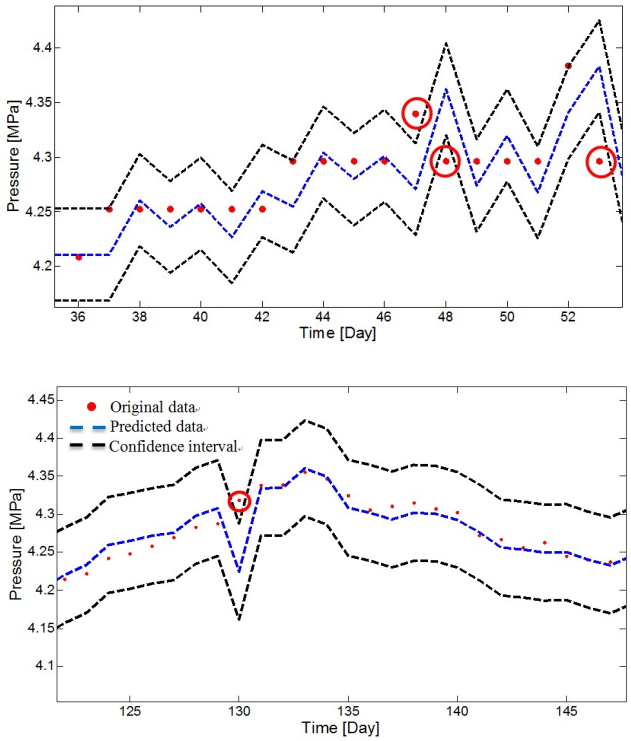

Figure 2-13 False alarm point monitored during sharp change for maximum pressure (upper) and mean pressure (lower)

Since all data points are known to be within normal condition, any data points out of the confidence interval are considered as false alarms. The false alarm rate for 50 days maximum pressure prediction is 0%; false alarm rate for 90 days maximum pressure prediction is 2.22%; the false alarm rate for 50 days mean pressure prediction is 0%; and the false alarm rate for 90 days mean pressure prediction is 1.11%. In addition, we combine both maximum and mean pressure to indicate the pressure characteristics, which means an abnormal pressure state of one day (consider both maximum pressure and mean pressure) should be defined as having abnormal points of both maximum pressure and mean pressure. Then there is no point out of respective confidence intervals, hence the false alarm rate is further reduced and gives better results.

Since the test data is normal data and our prediction indicates the normal degradation trend, it can also be inferred that if more out-of-bound points are detected during the life cycle of battery, the battery performance is drifted. The reasons may include accelerated degradation process due to faults, sensor degradation or drifting, or system instability. Hence, the percent of detected out-of-bound points during a period can be further used to help indicate and investigate the change of system.

2.6 Conclusions

We have investigated NiH_2 battery performance to help develop fault detection, reduce online false alarm rate, and predict the degradation process. ANN, ARMA and a hybrid model have been used to establish the data-driven model. The ARMA-ANN hybrid model provides the most accurate one-step-ahead prediction results in comparison with pure ARMA and ANN models. We have also developed statistical confidence interval for online fault detection. Results from both voltage and pressure measurements show reduced false alarm rate with 95% confidence interval. The method can also help reduce the false alarm rate without miss detection.

This chapter also discussed a multi-step-ahead prediction method for long-term degradation analysis of the NiH2 battery, by focusing on the pressure growth. The prediction results show the robustness and accuracy of the proposed model by comparing to the test data. In addition, further pressure behavior is predicted to provide health management support information.

CHAPTER 3

Parameter Estimation of Lithium-ion Battery Degradation Using Electrochemistry-Based Dual Models

3.1 Introduction

Lithium-ion (Li-ion) batteries are regarded as the most promising energy storage technology for new generation electric vehicles. Compared to alternative battery technologies, Li-ion batteries have much higher energy density, exhibit no memory effect and greater durability. However, due to the complexity and safety concerns of Li-ion batteries and customer habit, difficulty arises in properly estimating the battery energy level, e.g., the state of charge (SOC), monitoring the cell degradation processes, and predicting their remaining useful life (Armand and Tarascon, 2008). These features can be analysed by model-based methods.

The literature of Lithium-ion battery modelling is generally categorized into two classes: (1) equivalent circuit models (He, et al. 2012); and (2) physics-based models built upon electrochemical reaction (Chaturvedi, et al. 2010). The equivalent circuit models have limited usefulness for large scale energy applications (e.g., electric vehicles), which require higher accuracy compared to portable electronic applications, especially during operations involving both micro-cycling and deep cycling. In addition, many parameters are required to develop the equivalent circuit model and simulate the complete battery behaviour (Chaturvedi, et al. 2010). Furthermore, since the physics parameters turn into mere fitting parameters for the equivalent

circuit model, the intuition inside a battery is lost. Physics-based electrochemical models, including more detailed electrochemical phenomena in modeling, can not only resolve the above-mentioned difficulties, but can also improve the estimation and prediction performance of battery cell. Many studies have developed simplified electrochemical-based models that can provide robust and efficient estimation of battery cell state and parameters without the loss of computational efficiency (Sikha, et al. 2005, Smith, et al. 2010).

The precise estimation of SOC - a key battery indicator – is required in the electric vehicle applications. SOC indicates how much energy a battery has before it needs to be recharged (He, et al. 2012). SOC can reflect the energy level, and determine other output, such as estimated voltage. In addition, the SOC of a battery cell needs be determined to improve safety and efficiency during charging and discharging processes because accurate SOC estimation can help prevent over-charging and over-discharging conditions, and prevent different kinds of damage to the battery, and eventually extending the lifetime (Cheng, et al. 2011). Several techniques have previously been proposed to measure or estimate the SOC of battery single cell, each having its relative strength and limitation, as reviewed in (Zhang and Lee, 2011, Samadani, et al. 2012).

However, existing literature on electrochemistry-based SOC estimation focuses on single cell SOC estimation techniques for a short term, which could be inaccurate throughout the lifetime of the cell. Under different operating conditions, such as temperature, the depth of charge and discharge, aging effects on each individual cell can be different in terms of inner resistance, capacity and dynamics of chemical reactions. Besides, the driving behaviour may also cause different aging process among cells (Sarre, et al. 2004). All these differences may gradually increase over time and will be reflected by SOC divergence or the internal resistance divergence (Dubarry, et al. 2010). On the other hand, there are literatures showing the battery long-term

degradation, such as equivalent circuit based estimation to determine charge capacity fade and internal resistance increment as a degradation indicator (Plett, 2004); a charge-discharge capacity fade model based on the loss of active lithium ions due to solvent reduction reaction (Ning and Popv, 2004), but they were either based on simulation without real data verification, or lost most the actual information, which can be used to interpret the physical meaning of degradation process. There are few literatures showing the long-term cell degradation with electrochemistry-based model and verified by experimental results, hence, there is no sufficient information for an estimation of available energy and power and the level of cell deterioration indicated by changes in physical parameters over time. Therefore, for a reliable and accurate battery management system, the changes of SOC and parameters of a battery cell in the long term need to be accurately estimated for degradation monitoring. Methods have been provided, but with problems such as intensive computation, difficulty for online implementation in an automotive embedded system, and inaccuracy due to model constraints (Hu, and et al. 2012).

This chapter proposes a method to estimate both the SOC and long-term cell parameters of the battery by integrating a simplified electrochemical battery model and a Dual Extended Kalman Filter technique. The SOC and the film resistance of a single cell over its life time are estimated. The advantages of this proposed method are two-fold: (1) implementing physics-based models to provide physical interpretation of Lithium-ion battery cell, and (2) utilizing dual models to maintain the long-term accuracy of estimates. The estimation result from this method can be further extended to battery performance prediction and health management by analysing more long-term related parameters.

3.2 Electrochemical Battery Model

3.2.1 Chemical Reaction

The electrochemical battery model has been studied in the field of electrochemistry. In this chapter, the model is established based on the major components of positive material Cobalt: $LiCoO_2$. The overall chemical reaction for Li-ion battery formula is given by

$$LiCoO_2 + C \leftrightarrow Li_{1-k}CoO_2 + Li_kC \tag{3-1}$$

which can be derived into two electrode reactions. For positive side, Li^+ ions are extracted from $LiCoO_2$ by oxidation during charging and are inserted into $LiCoO_2$ by reduction during discharging.

$$LiCoO_2 \leftrightarrow Li_{1-k}CoO_2 + kLi^+ + ke^- \tag{3-2}$$

For negative side, Li^+ particles are inserted into Li_kC by reduction during charging and are extracted from Li_kC by oxidation during discharging.

$$kLi^+ + C + ke^- \leftrightarrow Li_kC \tag{3-3}$$

The mol fraction of Li^+ can be considered as the critical state of charge of the Li-ion battery, which is the electrode-average solid concentration at the electrolyte interface and can be transferred into the normally called state of charge.

3.2.2 Li-ion Diffusion and Concentration

The electrochemical principles are used to construct a physics-based model of a Li-ion battery. The one-dimensional model of a Li-ion battery considers the dynamics along only one axis (the horizontal *X*-axis) and neglects the dynamics along the rest two axes (*Y*-axis and *Z*-axis) (Danilov,

2011). This approximation is applicable to most cell structures with a large cross-sectional area and small currents. For example, the characteristic length scale of a typical Li-ion cell along the *X*-axis is in the scale of $100\mu m$, whereas the characteristic length scale for the remaining two axes is on the order of $1\mu m$ or more. To simplify the model, it is assumed that the average electrolyte concentration, c_e, is a constant. This assumption can be verified in (Santhanagopalan and White 2006) and is justified due to the insignificant difference (<5%) observed in the electrolyte concentration in the battery (Vidts, et al, 1995).

The Li-ion diffusion in electrolyte and electrode can be descried by Fick's first and second law.

$$J_i(x,t) = -D_i \frac{\partial c_i(x,t)}{\partial x} \tag{3-4}$$

$$\frac{\partial c_i(x,t)}{\partial x} = D_i \frac{\partial^2 c_i(x,t)}{\partial x^2} \tag{3-5}$$

Since the concentration in electrolyte is assumed to be constant along the *x* direction, the electrode diffusion in only one dimension is considered. By considering the material diffusion inside representative solid material particles for each electrode, the system from $x = 0$ to $x = r$ is divided into spatial elements of the thickness Δr. J_i is the flux of the diffusing elements at location x and time t, which can be determined by current *I* and its corresponding locations. D_i is the diffusion coefficient and $c_i(x,t)$ is the concentration of the diffusing element *i* at location *x* and time *t*. Initial and boundary conditions have to be defined for each diffusion problem in (3-8) and (3-9). In a linear diffusion, we have discretized form

$$\partial N_i = AD(c_i - c_{i-1})/\partial x \tag{3-6}$$

where N is the number of moles within the element and A is the area. Based on the spherical geometry, we can obtain

$$\frac{\partial c_i}{\partial t} = \frac{D}{\Delta r^2}\left(\frac{i-1}{i}c_{i+1} - 2c_i + \frac{i+1}{i}c_{i-1}\right) \tag{3-7}$$

At the two boundaries, we have

$$\frac{\partial c_1}{\partial t} = \frac{D}{\Delta r^2}(2c_2 - 2c_1) \tag{3-8}$$

$$\frac{\partial c_{n-1}}{\partial t} = \frac{D}{\Delta r^2}\left(\frac{n-2}{n-1}c_{n-2} - \frac{n-2}{n-1}c_{n-1}\right) + \frac{DJ}{\Delta r}\frac{n}{n-1} \tag{3-9}$$

Finally, the state space equation for linear diffusion is

$$\dot{c} = \frac{D}{\Delta r^2}A_s c + \frac{D}{\Delta r}\frac{n}{n-1}B_s J \tag{3-10}$$

The parameters A_s and B_s are determined by Eq. (3-9). This approximation leads to an average value of the solid concentration that can be related to the definition of battery SOC. Although this simplified model may result in a loss of information, it is efficient in control and estimation applications and still maintains a connection with the physical phenomena and dimensions.

The SOC is determined by the stoichiometry value μ_i in Eq. (3-11) and (3-12) (Domenico, 2010), where $\overline{c_s}$ is the average solid concentration and c_{smax} is the maximum solid concentration. Here, we assume that the maximum solid concentration is constant along the battery life cycle.

$$SOC(t) = \frac{(\mu - \mu_0)}{(\mu_1 - \mu_0)} \tag{3-11}$$

$$\mu = \frac{\overline{c_s}}{c_{smax}} \tag{3-12}$$

3.2.3 Butler-Volmer Current, Overpotential and Voltage Computation

The overall battery terminal voltage V is constructed in Eq. (3-13) by battery's open circuit voltage (OCV, E_{ocv}), overpotential (η), electrostatic potentials (φ), and film resistance (R_f) on the

electrodes surface. The details can be found in Danilov, 2011 . We also applied the average model in developing the electrochemical mechanism.

$$V = E_p - E_n = (E_{ocv,p} + \eta_p + \phi_p) - (E_{ocv,n} + \eta_n + \phi_n) - IR_f \tag{3-13}$$

The OCV can be determined based on empirical correlation described in (Doyle and Fuentes, 2003). The overpotential can be determined by Butler-Volmer current density while the electrostatic potentials are determined by the thickness of electrodes and separator. By substituting Eq. (3-14 through 3-18) into (3-13), we can develop the battery voltage.

$$\phi_p - \phi_n = \frac{\delta_p + 2\delta_{sep} + \delta_n}{2Ak_{ef}} \tag{3-14}$$

$$E_{ocv,p} = v_0 + v_1\theta + v_2\theta^{0.5} + v_3\theta^{-1} + v_4\theta^{1.5} + v_5 e^{v_6\theta + v_7} + v_8 e^{v_9\theta + v_{10}} \tag{3-15}$$

$$E_{ocv,n} = u_0 + u_1\theta + u_2\theta^2 + u_3\theta^3 + u_4\theta^4 + u_5\theta^5 + u_6\theta^6 + u_7 e^{u_8\theta} \tag{3-16}$$

$$\eta_p - \eta_n = \frac{RT}{\alpha nF} ln\left(\frac{j_p + \sqrt{{j_p}^2 + 4a^2 j_0^2}}{j_n + \sqrt{{j_n}^2 + 4a^2 j_0^2}}\right) \tag{3-17}$$

$$j_0 = \left(c_e(c_{se_{smax}}()^{\alpha}\right) \tag{3-18}$$

J_0 is the referenced current density determined by Li^+ concentrations at different stage (Vidts, et al. 1995). a is the Active surface area per electrode unit volume, and v and u are the coefficients for empirical correlation. Besides, δ is the thickness of electrode and separator. R is the inner resistance, R_f is the film resistance, A is the electrode plate area, and k_{eff} is the effective electrolyte phase diffusion conductivity (Domenico, et al, 2008).

Thus, the average Butler–Volmer current considers a representative solid material particle somewhere along the negative (n) and positive (p) electrodes. This simplified model has similarities with the "single-particle" model introduced in (Danilov, 2011). The diffusion

dynamics are approximated with a state space equation of first order ordinary differential equation, which has been described in above section, Eq.(3-10). Furthermore, in the electrode-average model, the cell voltage depends, through E_p and E_n, on the solid-electrode concentration instead of the average single-particle bulk concentration.

3.3 Extended Kalman Filter (EKF)

Extended Kalman filtering (EKF) is widely used to estimate system state and parameters for non-linear cell models by using a linearization process at every time step. The EKF method can automatically compute the dynamic battery cell "state" and its error bounds in real time based on real-time measurements. Usually, battery voltage, current, and temperature are measured with sensor noise. In this study, instead of deriving the SOC as the system state in EKF model directly, we use the solid concentration at the electrodes (c_{es}) as the system state to be determined. Solid concentration c_{es} is determined by the approximation analysis of Li-ion diffusion process in the previous section. The electrochemical model involves both system noise and sensor noise, w, and v, which are assumed to be zero-mean, Gaussian noises, respectively.

In section 3.2.2, the voltage is found to be a nonlinear function of Li-ion concentration. We use the voltage as the output in the EKF model. The EKF can then be implemented as:

$$\dot{x} = Ax + Bu + L(y - \hat{y}) \tag{3-19}$$

$$\hat{y} = V(x, u) \tag{3-20}$$

where $V(x, u)$ is determined by the solid concentration x (c_{se}) of the final segment in Eq. (3-13). A and B are the same matrix in Eq. (3-10). The procedure for Kalman gain calculation is shown below (Plett, 2004).

Initial condition (k = 0):

$$x_0{}^{+} = x_{initial}$$

$$\Sigma_{x,0}^{+} = (x_0 - x_0^{+})(x_0 - x_0^{+})^T$$

For k = 0, 1, 2, 3 …

Time update:

State: $L = \sum_{\hat{x}}^{-} \hat{C}^T [\hat{C} \sum_{\hat{x}}^{-} \hat{C}^T + \sum_v]^{-1}$

Error covariance: $\sum_{x,k+1}^{-} = A_k \sum_{x,k}^{+} A_{k-1}{}^T + \sum_w$

Kalman: $L_{k+1} = \sum_{x,k+1}^{-} C_{k+1}^T [C_{k+1} \sum_{\hat{x},k+1}^{-} C_{k+1}^T + \sum_v]^{-1}$

Measurement update:

State: $x_{k+1}^{+} = Ax_{k+1}^{-} + L_{k+1}[y_{k+1} - (Ax_{k+1}^{-} + Bu_k)]$

Error covariance: $\sum_{x,k+1}^{+} = (1 - L_{k+1} C_{k+1}) \sum_{x,k+1}^{-}$

Here, ∑w and ∑v are the covariance of noise w from system, and noise *v* from sensor. And the matrix C_k for the nonlinear system is shown below. The full derivation is not presented due to the equation complexity.

$$C_k = \frac{\partial V}{\partial x_k}|_{x_k = x_k{}^{-}} \tag{3-21}$$

$$C_k = \frac{\partial V}{\partial c_{s,p,(N-1)}} = \frac{\partial E_p}{\partial c_{s,p,(N-1)}} - \frac{\partial E_n}{\partial c_{se,n}} \frac{\partial c_{se,n}}{\partial c_{s,n,(N-1)}} \tag{3-22}$$

Figure 3-1 illustrates the discrete time EKF model. *x* and $\hat{y}$ are the estimated state and output, respectively. The input *u* is the current density in this case. For software computation implementation, the system is further transformed into discrete time form, which is shown below.

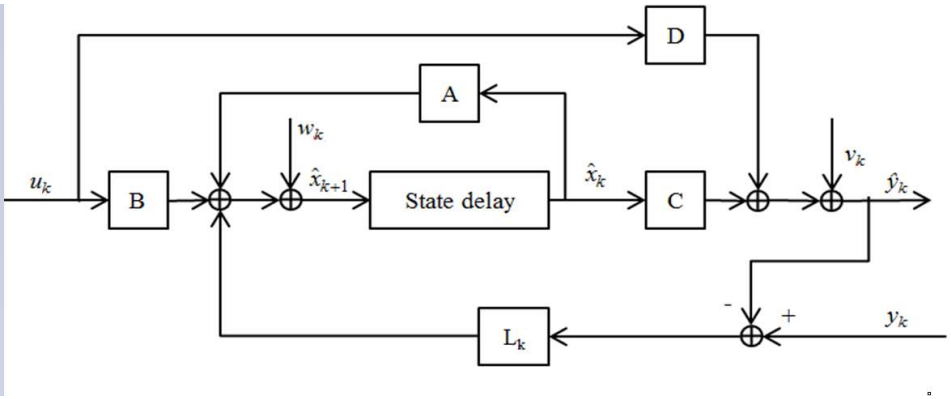

Figure 3-1 Discrete Time System with EKF

3.4 Dual Extended Kalman Filter (DEKF)

The state of charge (SOC), as one of the descriptive quantities of the present system state changes rapidly, while others may change slowly with time, such as inner resistance and cell capacity, which might change as little as 30% during 1000 cycles (Ning and Popov, 2004). These parameters decaying over time are often used to describe the state-of-health, and are important for cell degradation analysis and remaining useful life estimation.

The DEKF method is employed here to help estimate the values of state and parameters simultaneously, where two Kalman filters are implemented in the system shown below. The structure of the dual model is also described in Figure 3-2.

$$y_{k+1} = g(x_k, u_k, \theta_k) + v_k \tag{3-23}$$

$$z_{k+1} = g(x_k, u_k, \theta_k) + e_k \tag{3-24}$$

In this model, a critical cell parameter, cell film resistance, is tracked. The first system is described in 3.3, the second system in the discrete time form is determined below. Eq. (3-23) is the

same equation as Eq. (3-13), based on the concentration.

$$\theta_k = R_{f,k} \tag{3-25}$$

$$R_{f,k+1} = R_{f,k} + r_k \tag{3-26}$$

$$z_{k+1} = g(x_k, u_k, R_k) + e_k \tag{3-27}$$

Eqs. (3-25) and (3-26) show that the film resistance is generally time invariant, but it may vary slowly during long term due to gradual cell degradation during cycling. The process is modeled by r_k as the small degradation step. The output equation for the state-space model of true parameter dynamics is the cell output voltage estimate plus the estimation error e_k. Hence, in the dual model, voltage is the measurement for output update.

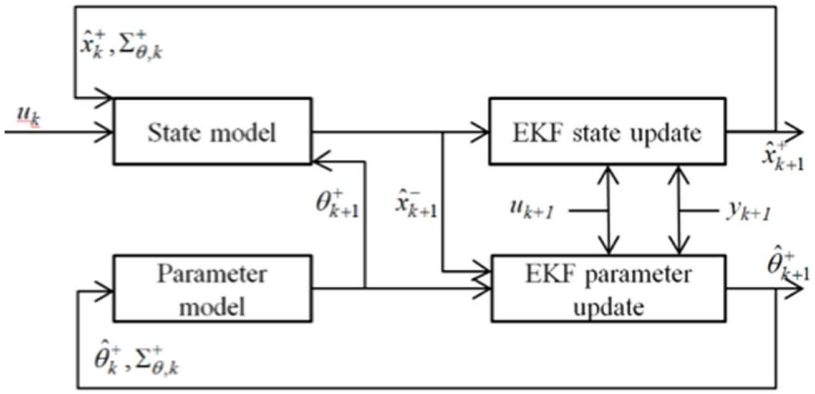

Figure 3-2 Discrete Time System with DEKF

3.5 Experiments and Discussion

In this section, we present the experiments[1] of the $LiCoO_2$ battery cell test and estimation results based on the proposed DEKF model. A single cell was tested in a climate chamber for 450 cycles. The battery temperature was maintained between 20°C and 29°C, while most of the time, the temperature is kept at 22°C. Due to the small variation, the temperature change has insignificant effect on the battery performance. The battery nominal voltage is 3.6V and for each discharging cycle, the battery was discharged from 4.1V (terminal voltage) to 2.5 V (terminal voltage), with a constant 1.5A current. For each charging cycle, the constant current constant voltage (CCCV) method was applied to protect battery from high voltage and overcharging damage. During the cycle, the battery was charged back to 4.2V (terminal voltage) by using constant 1.5A current and then was kept at constant voltage by reducing the current. To see the degradation effects over multiple cycles, we plot the battery measurement in the 1st cycle and the 401st cycle, as well as the SOC estimation in Figures 3-3 and 3-4. During the experiment, the current of discharging or charging processes were both recorded as positive values. High accuracy measurement sensors were applied to record the voltage and current.

From Figure 3-3, it is shown that at 401st cycle, the discharging time was reduced by 21%. This discharging capacity fading phenomenon can be viewed as one of the main indications of battery aging effect. Furthermore, the nominal voltage for the 401st cycle was also smaller than the

[1] This research is funded by NSF Industry & University Cooperative Research Program (I/UCRC) for Intelligent Maintenance Systems (IMS) at the University of Michigan. The authors would like to thank IMS center at the University of Cincinnati for providing experimental data.

one for the 1st cycle. This phenomenon can be physically described by film resistance increment on the surface of electrode particles. The long-term capacity fade and film resistance increment will be further discussed later.

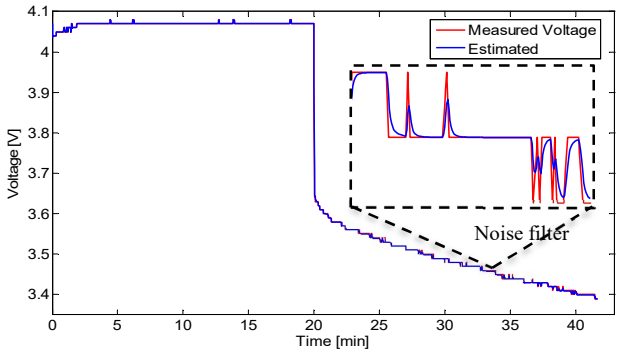

Figure 3-3 Short Term Voltage Estimation

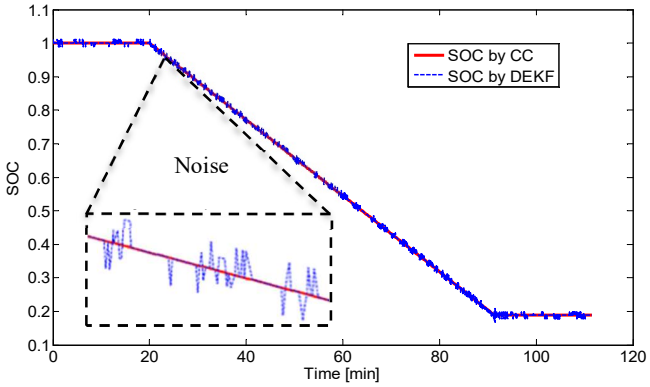

Figure 3-4 Short Term SOC Estimation

The results of short-term voltage and SOC estimation in one discharging cycle are shown in Figures 3-4 and 3-5. In Figure 3-4, the estimated voltage by using the DEKF is compared with the measurement. It can be observed that the estimate converges to the measurement and the noise variation is reduced by implementing Kalman Filter. In Figure 2-5, the SOC estimation is further compared with *coulomb counting* (CC) method. It can be observed that the estimated SOC converges to the CC results. During our experiment, the current was precisely controlled at 1.5A

and the SOC determined by the CC method is a linear line with no noise. We noted that the noise of SOC estimated by the DKEF is introduced by measured voltage. Here, we use the CC method conducted in ideal experimental environment to verify the DEKF method. It can be inferred that when there is noise in the current measurement in real applications, the DKEF SOC estimation will be more effective than the CC SOC estimation due to its noise filtering capability.

The discharging capacity for each cycle determined based on the CC methods and DEKF SOC changes are shown in Figure 3-5 Long-Term Capacity Fade Estimation. Though some large battery capacity recoveries are observed due to experimental interruption and variants, it can be concluded that the discharging capacity determined based on the DEKF is valid and effectively monitors the degradation process.

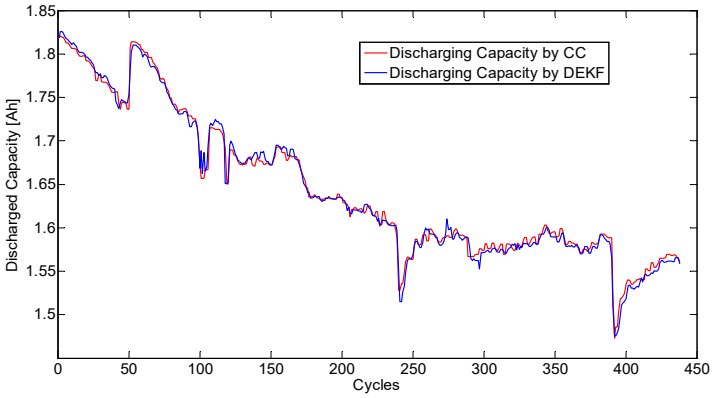

Figure 3-5 Long-Term Capacity Fade Estimation

To understand the cell degradation effects on the film resistance, we use the DEKF to estimate the long-term film resistance change. Since there is no way to directly measure the film resistance, an alternative method, *film growth rate method* (FGRM) (Moura, 2011) based on a first-principle battery model, is used to compare and verify the estimation performance of the proposed DEKF method. FGRM has been considered as the most efficient method in determining the film growth at solid electrolyte interphase (SEI), which is one of the main contributors to capacity fade and

battery age (Doyle, 2003). The single cell film resistance growth is determined by

$$R_{film}(x,t) = R_{SEI} + \frac{\delta_{film}(x,t)}{\kappa} \tag{3-28}$$

$$\frac{\partial \delta_{film}(x,t)}{\partial t} = -\alpha J(x,t) \tag{3-29}$$

where R_{SEI}, κ and α are the battery parameters. δ is the thickness of the layer. The comparison of per unit area film resistance determined by the DEKF and the FGRM is shown in Figure 3-7. The film resistance is averaged in each cycle to better demonstrate our result. In Figure 3-7, we observe that the film resistance growth estimates have similar values and same pattern as the FGRM. However, there is limitation by applying the FGRM to verify our simplified battery model due to some assumptions in the simplified electrochemical model. It is assumed that the maximum solid concentration is constant over the battery life cycle and the SOC is determined based on the 1st cycle of the battery. Due to the degradation effects, the speed of voltage drop during discharging will increase along its life cycle. The voltage-drop effects involve several parameter changes including film resistance, diffusion coefficient, material thickness and lithium concentration changes, but only the film resistance is considered in our simplified electrochemical model. Therefore, the film growth rate estimated upon the assumption might overestimate the film resistance. It is also shown that the estimation by the DKEF has larger values than that by the FGRM. One possible reason is that the first dynamic model embedded in the DKEF involves many parameters other than film resistance. Some of the parameters will also change through the cell life time, instead of keeping constant in the present model. This simplification could affect the accuracy of estimated parameters.

One advantage of the proposed DEKF over the FGRM is that DEKF can also be applied to estimate other cell parameters, even if we don't know the parameter aging mechanism, such as

lithium ions concentration reduction (Hu, et al. 2012). In other words, this comparison demonstrates that the DKEF is a useful technique for parameters tracking in the long run throughout the cell aging process, especially when the fundamental aging mechanisms of the parameters are not clearly understood.

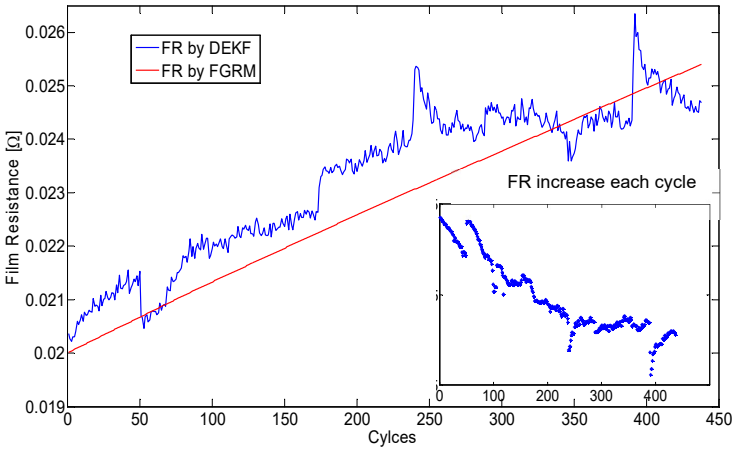

Figure 3-6 Long-Term Film Resistance Estimation

3.6 Conclusions and Future Work

This chapter proposed a method for estimating both the state of charge and cell parameters of a Li-ion battery cell over its lifetime using the Dual Extended Kalman Filters. To determine the state of charge accurately, the electrochemical model is developed to represent the cell dynamics, which is more advanced than equivalent circuit model. The experimental and simulation results show an efficient estimation and quick convergence of the SOC and robust estimation of parameters changing in the long run. The experimental and estimation results also show that the discharging capacity and film resistance determined based on the DEKF is valid and effectively represent the degradation process. It can also be inferred that if there is noise in the sensor measurement and battery system itself, the estimations based on the DEKF will be more accurate

than that based on the CC method due to the noise filtering capability and long-term parameter tuning function.

Comparing to the research done by Plett, (Plett, 2004), and Hu, (Hu, 2012), the DEKF with electrochemical model provide in-depth study of battery aging process as well as higher estimation robostness and accuracy.

Future work might investigate more cell parameters other than the film growth rate, if we have a better understanding of complicated aging effects on different parameters. A future study might also consider abrupt changes of parameters for accurate battery performance prognostics. The accuracy of the battery state and parameters estimation by applying the DKEF can be further improved at the cost of increased model complexity and computational effort.

NOMENCLATURE

Symbol	*Description*	*Unit*
a	Active surface area per electrode unit volume	cm^{-1}
c_i	Li-ion concentration	mol cm^{-3}
n	Particle coefficient	–
r	Particle radius	cm
A	Area	cm^2
D	Diffusion coefficient	–
E	Open circuit voltage	V
F	Faraday's constant	C mol^{-1}
I	Current	A
J	Butler–Volmer current density	A cm^{-3}
K_{ef}	Effective electrolyte phase diffusion conductivity	cm^2 s^{-1}
L	Kalman Gain	–
R	Gas constant	J K^{-1} mol^{-1}
R_f	Film resistance	Ω
T	Temperature	K
α	Change transfers coefficients	–
δ	thickness	cm
η	Overpotential	V
μ	Stoichiometry value	–
φ	Potential	V
$\sum$	Covariance	–

CHAPTER 4

Li-ion Battery Prognostics with Non-linear Degradation

4.1 Introduction

With the growth in battery-powered electric vehicle development, the lithium-ion battery plays a critical role in the reliability of vehicle systems. In order to provide timely maintenance and replacement of battery systems, it is necessary to develop a reliable and accurate battery health management system that takes a prognostic approach. Therefore, this chapter focuses on two main methods to determine a battery's health with non-linear degradation: (1) Battery State-of-Health (SOH) monitoring and (2) Remaining Useful Life (RUL) prediction. Both of these are calculated by using a filter algorithm known as the Support Vector Regression-Particle Filter (SVR-PF). Models for battery SOH monitoring based on SVR-PF are developed with novel capacity degradation parameters introduced to determine battery health in real time.

Many research papers in the field of battery remaining useful life (RUL) prediction are principally based on the development of prognostics tools. (Liu et al. 2011) applied a regularized auxiliary particle filter algorithm on battery SOH estimation and RUL prediction, and made comparisons to an auxiliary particle filter. (Eddahech et al. 2011) used battery electrochemical impedance spectroscopy (EIS) data to predict Lithium-ion battery RUL. (Nuhic et al. 2013) developed an algorithm based on Support Vector Machine (SVM) to estimate the SOH and RUL of lithium-ion batteries. A simplified electrochemical model was developed by (Prasad et al. 2013)

to identify the key aging parameters of a lithium-ion battery. (Widodo et al. 2011) applied both SVM and Relevance Vector Machine (RVM) on battery health monitoring and prognostics. They compared the results between these two kernel machines, thereby demonstrating that RVM had better predictive capability than SVM. (He et al. 2011) estimated battery health condition first by using the Particle Filter (PF), where the initial states for the PF were provided by Dempster-Shafter theory, then the parameters reflecting battery health condition generated from monitoring battery SOH were used to predict the battery RUL. A dual filter consisting of a Kalman Filter and Unscented Kalman Filter (UKF) was introduced by (Andre et al. 2011) to estimate lithium-ion battery State-of-Charge (SOC) and SOH. (Chiang et al. 2011) established an adaptive control approach to model a lithium-ion battery by calculating both the Open-Circuit Voltage (OCV) and internal resistance to estimate the battery SOC and SOH. (Chen et al. 2013) analyzed lithium-ion battery SOH through a Genetic Algorithm (GA), the temperature influence was also considered in their research work to improve the robustness and precision of SOH estimation.

(Schmidt et al. 2010) developed an online approach for estimating the residue power and capacity of a lithium-ion battery during operation. (Plett, 2004) published a series of papers on the Extended Kalman Filter (EKF) based battery management system for a hybrid electric vehicle battery. (Wang et al. 2013) developed a prognostic method to estimate the SOH and RUL of lithium-ion batteries based on Relevance Vector Machine (RVM) using an offline algorithm. (Saha et al. 2009) focused on monitoring battery SOH and RUL prediction by using the RVM and PF. Research work of (Takeno et al. 2004) showed that the linear correlation between capacity and impedance of Lithium-ion battery, and the correlation was largely unaffected by the degree of charge. (Orchard et al. 2013) presented a lithium-ion battery SOC prediction method based on PF.

Miao et al. predicted Lithium-ion battery RUL by using Unscented Particle Filter (UPF) and analyzing both predicted RUL and its distribution.

In the light of the previous works, we address two issues:

(1) Above literature reviews showed the battery capacity degradation was correlated with impedance data extracted from EIS, moreover, (Saha et al. 2009, Takeno et al. 2004) claimed the correlation was linear and used a linear regression algorithm to estimate it. We discovered that impedance data extracted from EIS could provide us new parameters to analyze battery degradation. These degradation parameters should be estimated through an online process such that the real time battery health condition can be monitored. Similar parameters are estimated by the linear regression algorithm in (Saha et al. 2009, Takeno et al. 2004)

(2) Several researchers predicted the battery RUL probability distribution by estimating parameters with run to failure test. However, the RUL prediction is a multi-step ahead process, the parameters distribution is not updated.

In this chapter, we build novel battery SOH monitoring models to analyze the proposed degradation parameters and develop a new approach to predict the RUL by updating its probability distribution. Moreover, the Support Vector Regression-Particle Filter (SVR-PF) algorithm is implemented to make improvement over the standard PF, which has the degeneracy phenomenon. The results show that together with the aging parameters (Saha et al. 2009) the degradation parameters accurately reflect the real time health condition of the battery and insure that an accurate RUL prediction can be calculated, and the SVR-PF shows improved estimation and prediction capability than the standard PF. The percentage of nominal capacity is considered as the parameter that reflects the battery SOH.

4.2 Particle Filter and Support Vector Regression-Particle Filter

4.2.1 Particle Filter

Particle Filter (PF) is a general algorithm based on the recursive Bayesian estimation (Sorenson, 1971), which uses the idea of the Monte Carlo method to draw samples (also called particles) from posterior distribution and assigns a weight to each particle (Carpenter et al. 1999).

Compared to the Kalman Filter, which only focuses on linear systems and Gaussian noise (Kalman, 1960), a particle filter focuses on a more general situation where the system can be nonlinear, and the noise distribution can be non-Gaussian. The system state space model for PF is:

$$\begin{cases} x_k = f(x_{k-1}, v_{k-1}) \\ z_k = h(x_k, n_k) \end{cases} \tag{4-1}$$

where x_k represents the system states and z_k represents either the measurements or the system outputs, v_{k-1} and n_k are system noise and measurement noise, respectively, and both can be either Gaussian or non-Gaussian.

Suppose we know the prior distribution $p(x^i_{0:k-1}|z_{1:k-1})$ and have already drawn *N* samples from the posterior distribution from system (4-1). The approximation of the posterior distribution is:

$$p(x_{0:k}|z_{1:k}) \approx \sum_{i=1}^{N} w_k^i \delta\left(x_{0:k} - x^i_{0:k}\right) \tag{4-2}$$

where $\{x_k^i\}$ represents the samples (i.e., the particles), $\{w_k^i\}$ represents the sample weights and $\sum_i^N w_k^i = 1$. A higher weight indicates a higher probability. $\delta()$is the Dirac-Delta function.

Because it is hard to sample directly from a posterior distribution, we use another technique known as Importance Sampling, which draws samples from the importance distribution and has this form:

$$q(x_{0:k}|z_{1:k}) \approx \sum_{i=1}^{N} \delta(x_{0:k} - x_{0:k}^{i}) \tag{4-3}$$

If we substitute the importance distribution (4-3) into (4-2), the weight update is given by:

$$w_k^i = \frac{p(x_{0:k}^i|z_{1:k})}{q(x_{0:k}^i|z_{1:k})} \tag{4-4}$$

If the importance distribution (4-2) can be decomposed to:

$$q(x_{0:k}|z_{1:k}) = q(x_k|x_{0:k-1}, z_{1:k})q(x_{0:k-1}|z_{1:k-1}) \tag{4-5}$$

We can have the weight renewal equation based on Bayesian estimation:

$$\begin{aligned} w_k^i &= \frac{p(z_k|x_k^i)p(x_k^i|x_{k-1}^i)p(x_{0:k-1}^i|z_{1:k-1})}{q(x_k^i|x_{0:k-1}^i, z_{1:k})q(x_{0:k-1}^i|z_{1:k-1})} \\ &= w_{k-1}^i \frac{p(z_k|x_k^i)p(x_k^i|x_{k-1}^i)}{q(x_k^i|x_{0:k-1}^i, z_{1:k})} \end{aligned} \tag{4-6}$$

where $p(z_k|x_k^i)$ is the likelihood function, $p(x_k^i|x_{k-1}^i)$ is the state transfer distribution, if the system (4-1) follows the Markovian process, we can simplify the weight renewal equation (4-6) to

$$w_k^i = w_{k-1}^i \frac{p(z_k|x_k^i)p(x_k^i|x_{k-1}^i)}{q(x_k^i|x_{k-1}^i, z_k)} \tag{4-7}$$

And if we choose state transfer distribution to be the importance distribution:

$$q(x_k^i|x_{k-1}^i, z_k) = p(x_k^i|x_{k-1}^i) \tag{4-8}$$

The weight update equation can be simplified to (4-9), in which the likelihood function $p(z_k|x_k^i)$ and the prior weights are used to update the new weights:

$$w_k^i = w_{k-1}^i p(z_k|x_k^i) \tag{4-9}$$

Resampling is used to avoid the problem of degeneracy of the PF algorithm. Without resampling, after a few iterations, some of the particle weights will tend toward zero, so efforts for calculating these weights becomes unnecessary. This condition is known as the degeneracy phenomenon (Saha et al. 2009).

The standard approach for the degeneracy phenomenon is to remove the small weight particles, and duplicate large weight particles to renormalize the distribution and set the weights of all the particles to $1/N$ (N is the number of particles). This is the resampling algorithm of the standard PF.

The threshold of resampling is defined as effective sampleN_{eff}, and is calculated by:

$$N_{eff} = \frac{N}{1+var(w_k^i)} \approx \frac{1}{\sum_{i=1}^{N}(w_k^i)^2} \tag{4-10}$$

4.2.2 Support Vector Regression-Particle Filter (SVR-PF)

The standard PF algorithm for avoiding the degeneracy phenomenon by eliminating small weight particles and duplicating large weight particles will cause the loss of particle diversity, this may result in most particles gathering around the larger weighted ones, and therefore the degeneracy phenomenon will still exist. In order to avoid this problem, a new resampling algorithm is introduced to rebuild a posterior distribution (4-1), and is known as SVR (Bishop, 2006), which can avoid the degeneracy phenomenon and keep the diversity of particles. (Jiang et al. 2009)

introduced a basic algorithm on SVR-PF and applied it to nonlinear systems. (Kabaoglu, 2009) applied SVR-PF to the problem of direction-of-arrival multiple target tracking. (Zhu et al. 2005) improved the efficiency of visual tracking system by SVR-PF, the basic algorithm was also introduced in their research work.

The fundamental idea that rebuilds posterior distributions by SVR is known as an optimization problem using a regularized functional with constraints (Vapnik, 1995), which has the following form:

$$\begin{cases} \Omega = (f, f)_H \\ \text{s.t.} \sup\limits_x |F(x) - F_l(x)| = \sup\limits_x \left| F_l(x) - \int_{-\infty}^{x} f(t)dt \right| = \sigma_l < \varepsilon \end{cases} \tag{4-11}$$

where $\Omega = (f, f)_H$ is the regularized function defined in Hilbert space and is generated by σ_l. σ_l is the error or distance between distribution function $F(x)$ and its estimation $F_l(x)$. ε is the constraint.

$f(x)$ is the probability density function (PDF) of estimate distribution $F_l(x)$. We only need to consider points $x_i (i = 1,2, \dots, m)$ in the particle set, thus (4-11) can be simplified to:

$$\max_i \left| F_l(x) - \int_{-\infty}^{x} f(t)\, dt \right|_{x=x_i} = \sigma_l < \varepsilon \tag{4-12}$$

If we describe the PDF $f(x)$ by kernel functions:

$$f(x) = \sum_{i=1}^{m} \beta_i K(x_i, x) \tag{4-13}$$

$K(x_i, x) = \varphi^T(x_i)\varphi(x)$ is the kernel function, which satisfies Mercer's condition (Ferreira, 2009). Then we can get the regularized function:

$$\Omega(f) = (f, f)_H = \sum_{i=1}^{m} \sum_{j=1}^{m} \beta_i \beta_j K(x_i, x_j) \tag{4-14}$$

The posterior distribution estimation problem can be described as a constraint optimization problem:

$$\begin{cases} min\, W_p(\beta) = \sum_{i=1}^{m}\sum_{j=1}^{m}\beta_i\beta_j K(x_i, x_j) \\ \text{s.t.} \max_i \left| F_i(x) - \sum_{j=1}^{m}\beta_j \int_{-\infty}^{x} K(x_j, t)dt \right|_{x=x_i} = \sigma_l \end{cases} \tag{4-15}$$

set $y_i = F_i(x_i), w = [\beta_1, \beta_2, \dots, \beta_m]^T$, $z_j(x) = \int_{-\infty}^{x_j} K(x,t)dt$, $z_i = (z_i(x_1), z_i(x_2), \dots, z_i(x_m))$, ξ_i and ξ_i^* are non-negative slack variables, Eq. (4-15) can be transferred to a quadratic programming problem:

$$\begin{cases} min\, J(w, \xi_i, \xi_i^*) = \frac{1}{2}w^T w + C(\sum_{i=1}^{m}\xi_i + \sum_{i=1}^{m}\xi_i^*) \\ \text{s.t} \quad w^T z_i - y_i \le \sigma_l + \xi_i \\ \qquad y_i - w^T z_i \le \sigma_l + \xi_i^* \\ \qquad \xi_i, \xi_i^* \ge 0, i = 1,2, \dots m \end{cases} \tag{4-16}$$

where *C* is the penalty coefficient. By introducing Lagrange coefficients a_i, a_i^* to (4-16), we get:

$$\begin{cases} max\, W(a_i, a_i^*) = -\frac{1}{2}\sum_{i=1}^{m}\sum_{j=1}^{m}(a_i^* - a_i)(a_j^* - a_j)(z_i^T z_j) - \sigma_l\sum_{i=1}^{m}(a_i^* + a_i) + \sum_{i=1}^{m} y_i(a_i^* - a_i) \\ \text{s.t.} \sum_{i=1}^{m}(a_i^* - a_i) = 0, 0 \le a_i, a_i^* \le C, i = 1,2, \dots, m \end{cases} \tag{4-17}$$

Now we derive the solution of (4-17) as follows:

$$\beta_j = \sum_{i=1}^{m}(a_i^* - a_i)z_i(x_j) \tag{4-18}$$

In (4-18), x_i is the Support Vector and is the corresponding parameter of non-zero coefficients a_i^*, a_i. Substituting (4-18) into (4-13), we can transform the solution of the optimization problem to a posterior distribution estimation.

From the discussion above, the new PF algorithm can be modified by incorporating SVR and can be described as follows: When the effective sample N_{eff} falls below the threshold, a resampling of the posterior distribution using the SVR algorithm occurs. The two training pairs

are particle x_k^i and its corresponding weight $w_k^i = F_l(x_k^i)$. These pairs are used to rebuild the resampling posterior distribution. The procedure for the SVR-PF method is shown in Figure 4-1. $\tilde{x}_k^1, \ldots \tilde{x}_k^m$ and $\tilde{w}_k^1, \ldots \tilde{w}_k^m$ represent the rebuilt particles and weights respectively.

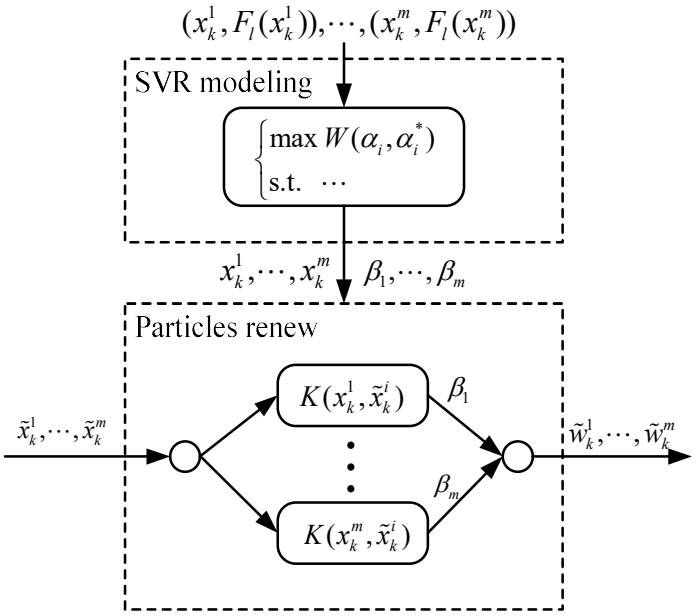

Figure 4-1 Fundamental illustration of SVR-PF

4.3 Circuit Model for a Lithium-ion Battery

This chapter uses battery capacity and impedance data, which are collected from second generation, Gen 2, 18650-size lithium-ion cells produced by Idaho National Laboratory (Goebel, 2008). The experiment ran at room temperature (24 degree Celsius). Charging was carried out in a constant current (CC) mode at 1.5A until the battery voltage reached 4.2V and then continued in a constant voltage (CV) mode until the charge current dropped to 20mA. Discharge was carried out at a constant current (CC) level of 2A until the battery voltage fell to 2.7V, 2.5V and 2.2V for batteries 5, 6 and 7, respectively. Impedance measurement were carried out through an

electrochemical impedance spectroscopy (EIS) frequency sweep from 0.1Hz to 5kHz. Repeated charge and discharge cycles resulted in accelerated aging of the batteries while impedance measurements provided insight into the internal battery parameters that changed as aging progresses. The experiment stopped when the battery reached its End-of-Life (EOL). The EOL threshold for each battery was different. In this experimental study the EOL threshold for batteries 5 and 6 was 70% of nominal capacity, while for battery 7 it was set at 74.5% nominal capacity.

Impedance data extracted from EIS is a good indicator for determining battery SOH. When a battery ages its impedance degrades as a function of time (Goebel, 2009; Zhang et al. 2000; Eddahech, 2012). Extracted impedance data can be analyzed based on the equivalent circuit for a single cell as shown in Figure 4-2. The major impedance data we need for RUL estimation are R_e and R_{ct}, which are electrolyte resistance and charge transfer resistance respectively (Goebel, 2009).

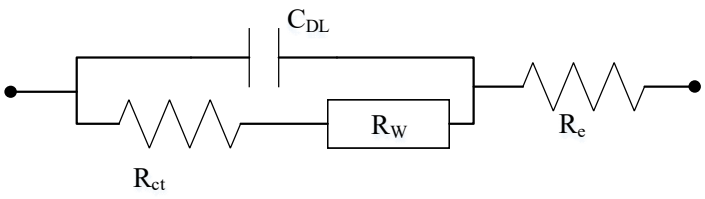

Figure 4-2 Equivalent circuit for single cell of battery impedance (Goebel, 2009)

The battery capacity (Ah) and impedance (Ohm) over cycle number are shown in Figure 4-3. The capacity of all three batteries decreases over charge-discharge cycles while battery impedance R_e and R_{ct} increase over cycles in a similar pattern.

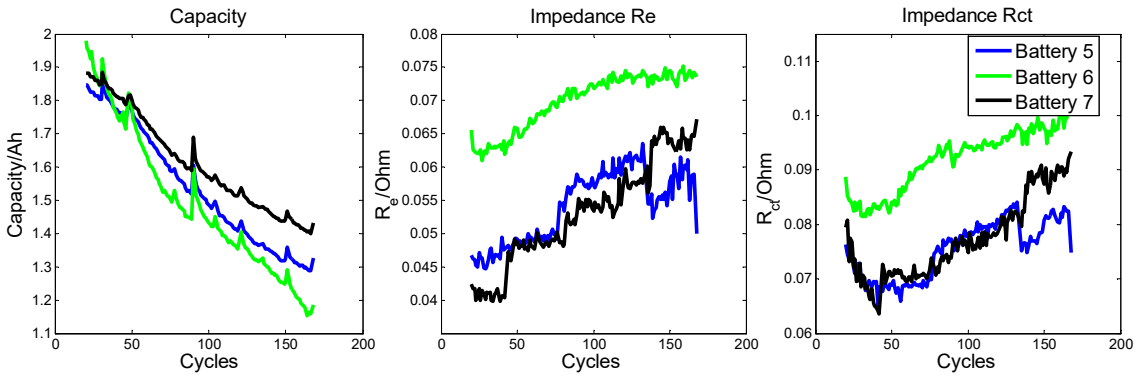

Figure 4-3 Battery Capacity and Impedance versus Cycle Number

4.4 Models for Battery SOH Monitoring

The battery SOH monitoring method is processed online and reflects the real time battery health condition using: (1) aging parameters (Saha, 2009) that provide the impedance aging trend versus time; and (2) degradation parameters that reflect battery capacity degradation through the impedance data.

The method is composed of three processes: (1) estimating the aging parameters and smoothing of the data, (2) developing the battery degradation model to estimate the proposed degradation parameter, and (3) detecting battery capacity degradation. Process (3) operates in parallel with processes (1) and (2) and provides a terminate signal when the battery SOH degrades below the RUL threshold value. The battery RUL threshold value in this chapter is defined as the percentage of battery nominal capacity and is set at a percentage of nominal capacity that is greater than the EOL threshold. SOH monitoring stops and RUL prediction begins when battery capacity degrades below the RUL threshold.

The processes of battery SOH monitoring are shown in Figure 4-4.

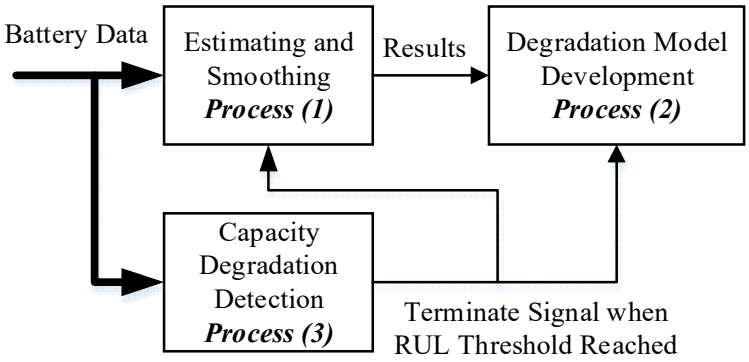

Figure 4-4 Diagram of battery SOH monitoring

4.4.1 Model for Battery Aging Parameter Estimation

The time dependent aging of impedance is observed by (Goebel, 2009; Zhang et al. 2000; Eddahech, 2012), it is modeled by an exponential function (Saha, 2009):

$$R=R0exp(\lambda Rt) \tag{4-19}$$

where R represents R_e or R_{ct}, R_0 is a constant, λ_R is the aging parameter, which is estimated through the PF.

Taking advantage of equation (4-19), we build a novel battery state space model using the SVR-PF in order to estimate the battery aging parameters. Besides, the experimental impedance data is also recursively smoothed:

$$\begin{cases} x_{1,k} = x_{1,k-1} + v_{1,k-1} \\ x_{2,k} = x_{2,k-1} + v_{2,k-1} \\ x_{3,k} = x_{3,k-1}\, exp(\, x_{1,k-1}\Delta k) + v_{3,k-1} \\ x_{4,k} = x_{4,k-1}\, exp(\, x_{2,k-1}\Delta k) + v_{4,k-1} \end{cases}$$

$$\begin{cases} z_{1,k} = x_{3,k} + n_{1,k} \\ z_{2,k} = x_{4,k} + n_{2,k} \end{cases} \tag{4-20}$$

where $x_{1,k}$ and $x_{2,k}$ represent the aging parameters λ_{R_e} and $\lambda_{R_{ct}}$, respectively, which are to be estimated. $x_{3,k}$ and $x_{4,k}$ represent the impedance R_e and R_{ct}, respectively, which are to be smoothed. $v_{1,k}$, $v_{2,k}$, $v_{3,k}$ and $v_{4,k}$ denote the state noise. $z_{1,k}$ and $z_{2,k}$ are outputs or measurements. $n_{1,k}$ and $n_{2,k}$ are output noise.

Data estimating and smoothing results for model (4-20) are now applied so that a degradation model parameter can be estimated in the following section.

4.4.2 Degradation Model – Degradation Parameters Estimation

The purpose of degradation model is to reflect the battery SOH. Based on the analysis in (Goebel, 2009), the capacity *C* degradation is linearly correlated with the sum of the impedance $R_e + R_{ct}$, and can be modeled by:

$$C = \alpha(R_e + R_{ct}) + \beta \tag{4-21}$$

where *C* represents the capacity, α and β are degradation parameters.

From equation (4-21), we can now determine the battery degradation model:

$$\begin{cases} \alpha_k = \alpha_{k-1} + v_{1,k-1} \\ \beta_k = \beta_{k-1} + v_{2,k-1} \end{cases}$$

$$C_k = \alpha_k(R_{e_k} + R_{ct_k}) + \beta_k + n_k \tag{4-22}$$

In this model, states α_k and β_k are degradation parameters, C_k represents battery capacity, R_{e_k} and R_{ct_k} are the smoothed impedance from the model (4-20), $v_{1,k}$, $v_{2.k}$ and n_k are noise.

4.5 Battery Remaining Useful Life Prediction

The prediction of RUL is based on the real-time battery health condition. When the RUL threshold value criterion is met, the SOH monitoring method stops, and the current battery health condition parameters are recorded. Refer to the analysis in the previous section, the battery capacity degradation is linearly correlated with the sum of the impedance (eq. (4-22)), therefore the impedance is predicted first to provide basic trend of the capacity degradation, the battery capacity is then predicted to calculate the RUL.

The aging parameters are used to predict the impedance. Suppose the RUL criterion is met at cycle *N*, the battery RUL given in cycle is *L* and $\hat{R}_e$, $\hat{R}_{ct}$ represent predicted impedance, we have:

$$\hat{R}_{e,N+m} = R_{e,N}\, exp(\lambda_{R_e,N} m). m = 1, \dots, M. M \geq L \tag{4-23}$$

$$\hat{R}_{ct,N+m} = R_{ct,N}\, exp(\lambda_{R_{ct},N} m). m = 1, \dots, M. M \geq L \tag{4-24}$$

In these equations, $R_{e,N}$, $R_{ct,N}$ are smoothed impedance at cycle *N* and $\lambda_{R_e,N}$, $\lambda_{R_{ct},N}$ are estimated aging parameters at cycle *N*.

The degradation parameters are embedded in the model to predict the battery capacity with the SVR-PF algorithm. Because the prediction is a multi-step ahead process, the estimated particles weights at the last cycle of SOH monitoring are not able to reflect the distribution of RUL at latest time step. This model is also built for updating the RUL distribution, which is:

$$\begin{cases} \lambda^*_{Re,k+1} = \lambda^*_{Re,k} + v^*_{1,k} \\ \lambda^*_{Rct,k+1} = \lambda^*_{Rct,k} + v^*_{2,k} \\ R^*_{e,k+1} = R^*_{e,k}\, exp(\lambda^*_{Re,k}\Delta k) + v^*_{3,k} \\ R^*_{ct,k+1} = R^*_{ct,k}\, exp(\lambda^*_{Rct,k}\Delta k) + v^*_{4,k} \\ C^*_{k+1} = \alpha_N(R^*_{e,k+1} + R^*_{ct,k+1}) + \beta_N \end{cases}$$

$$\begin{cases} \hat{R}_{e,k} = R^*_{e,k} + n^*_{1,k} \\ \hat{R}_{ct,k} = R^*_{ct,k} + n^*_{2,k} \end{cases} \tag{4-25}$$

In this model, parameters with * represent predicted parameters. α_N, β_N are estimated degradation parameters at cycle *N*. Model measurements $\hat{R}_e$, $\hat{R}_{ct}$ are predicted impedance from (4-23) and (4-24). Initial states particles are the recursively calculated results at the last cycle of SOH monitoring method. Prediction starts at time step $k = N$.

The capacity prediction process stops when the EOL threshold criterion is met, and the RUL is then calculated. The results provide not only the estimation value, but also the approximate probability distribution. Suppose the EOL threshold is met at cycle N_{EOL}, L^* is predicted RUL, $\{L^{*i}\}$ are the estimated RUL particles, which has the number of Q and $\{w^{*i}_{N_{EOL}}\}$ are the particle weights. We have the RUL value and distribution:

$$\overline{L^*} = \sum_{i=1}^{Q} w^{*i}_{N_{EOL}} L^{*i} = N_{EOL} - \tag{4-26}$$

$$P(L^*) = \sum_{i=1}^{Q} w^{*i}_{N_{EOL}} \delta(L^* - L^{*i}) \tag{4-27}$$

Including the SOH method, the whole process is illustrated in Figure 4-5:

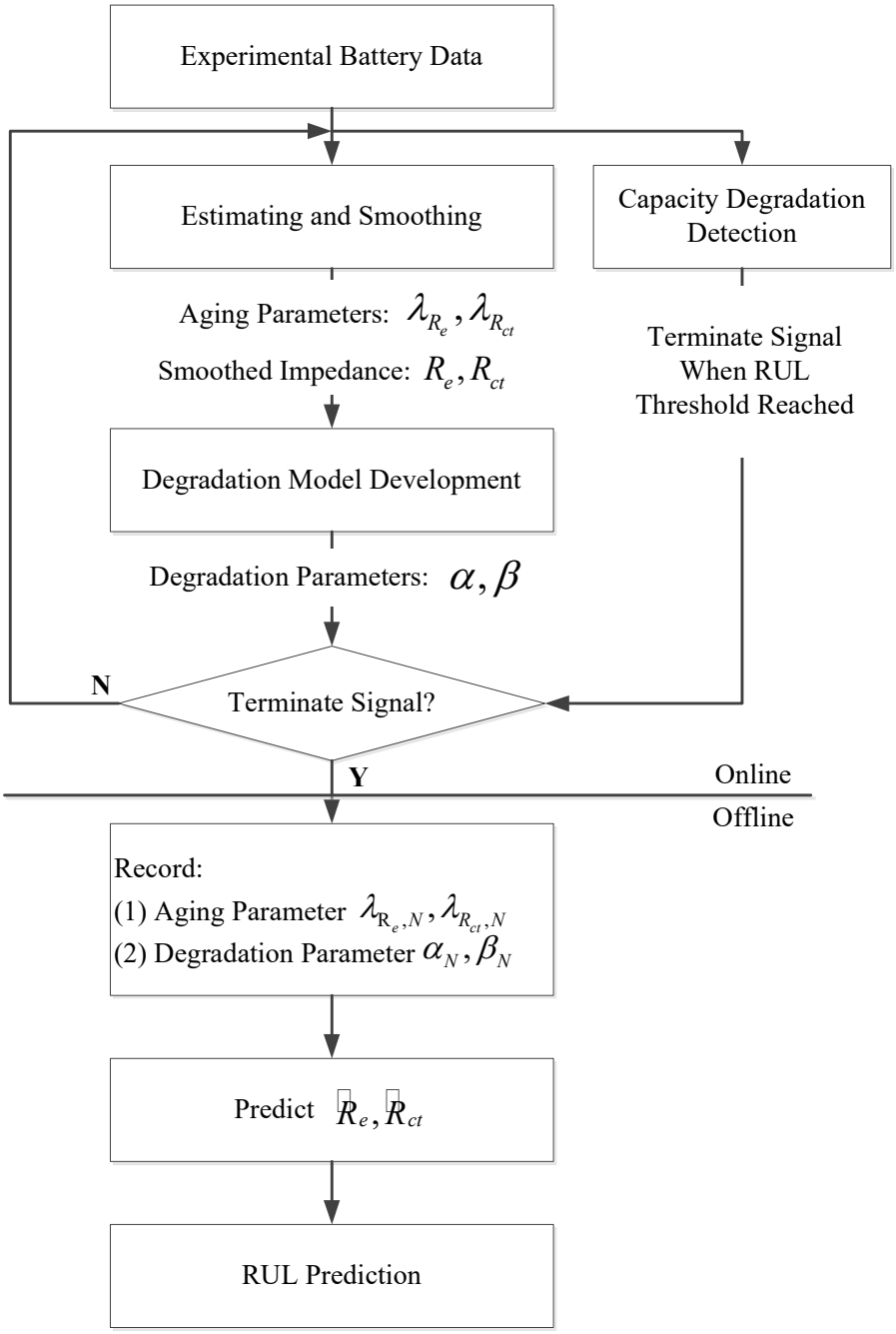

Figure 4-5 Flow chart of battery SOH monitoring and RUL prediction

4.6 Results – Comparing SVR-PF to PF

For the purpose that develops an online SOH monitoring method and avoids using post-processed data, the data of battery 6 is processed beforehand by using curve fitting algorithm to provide initial state of PF and SVR-PF, and the data of batteries 5 and 7 is applied in simulation.

4.6.1 Battery SOH Monitoring

Set the RUL threshold value of battery 5 to 80% nominal capacity, and 85% for battery 7. The battery SOH monitoring is calculated by SVR-PF and standard PF as shown in Figure 4-6. The mean squared error (MSE) of the results is shown in Table 4-1.

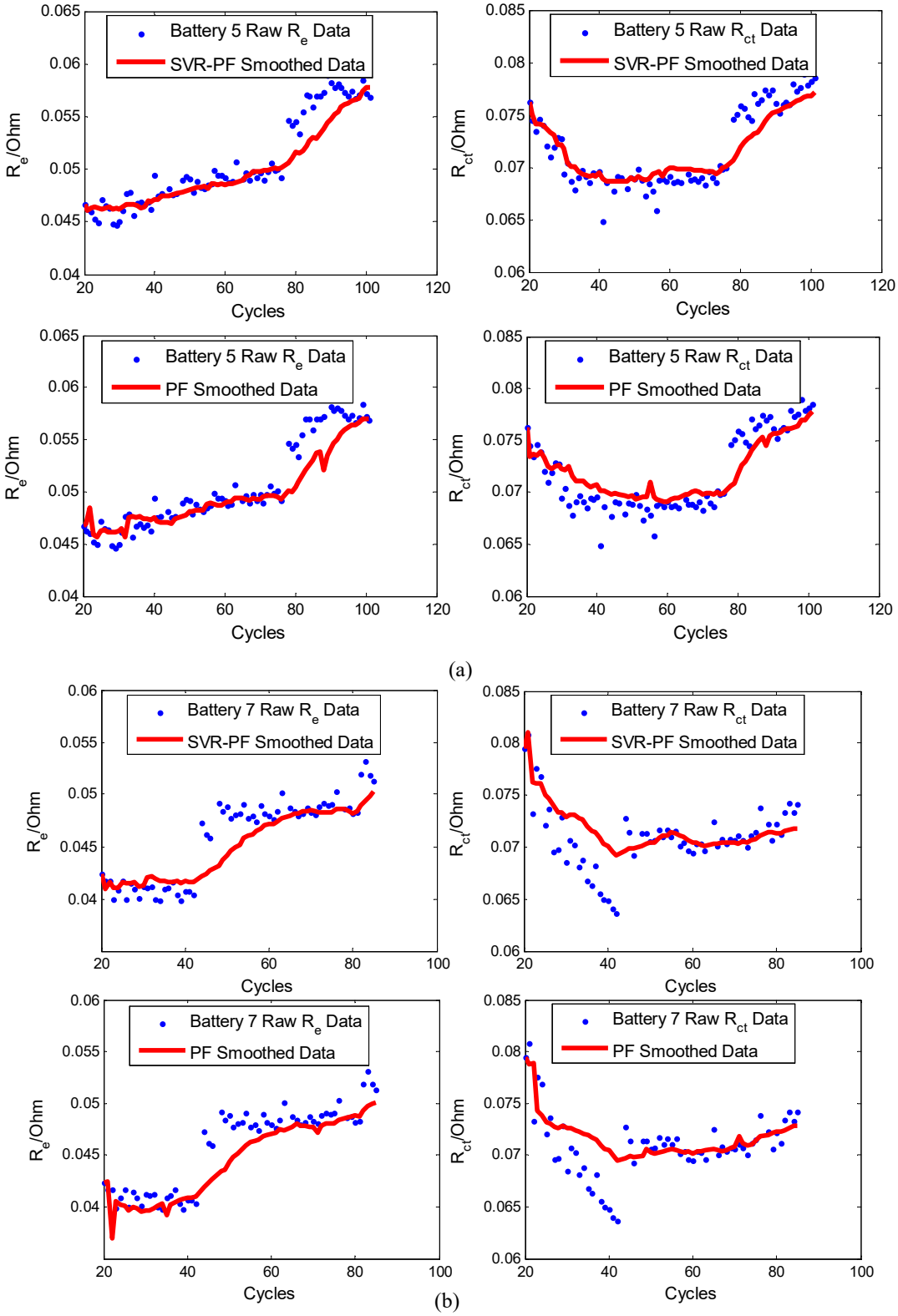

Figure 4-6 (a) Battery 5 and (b) battery 7 smoothing results from SVR-PF and PF

Table 4-1 Mean Squared Error of SVR-PF and PF Smoothed Performance

	Battery 5		**Battery 7**	
	R_e	R_{ct}	R_e	R_{ct}
SVR-PF	2.47×10^{-6}	4.58×10^{-4}	3.05×10^{-6}	6.15×10^{-4}
PF	5.81×10^{-6}	6.36×10^{-4}	5.27×10^{-6}	8.96×10^{-4}

To evaluate the performance of the SVR-PF method, we also apply the standard PF algorithm on the same set of batteries. By comparing the results from SVR-PF data tracking with PF data tracking, we observe that SVR-PF more accurately track results than PF because Mean Squared Errors (MSE) are much smaller, as shown in Table 4-1.

4.6.2 Remaining Useful Life Prediction

Next we investigate the battery RUL prediction. Set the RUL threshold value to 80% nominal capacity for battery 5, and to 85% for battery 7. The predicted battery capacity and RUL distribution for batteries 5 and 7 are shown in Figure 4-7 and Figure 4-8, respectively. Because we use random variables to generate initial particles, the simulation is repeated three consecutive times.

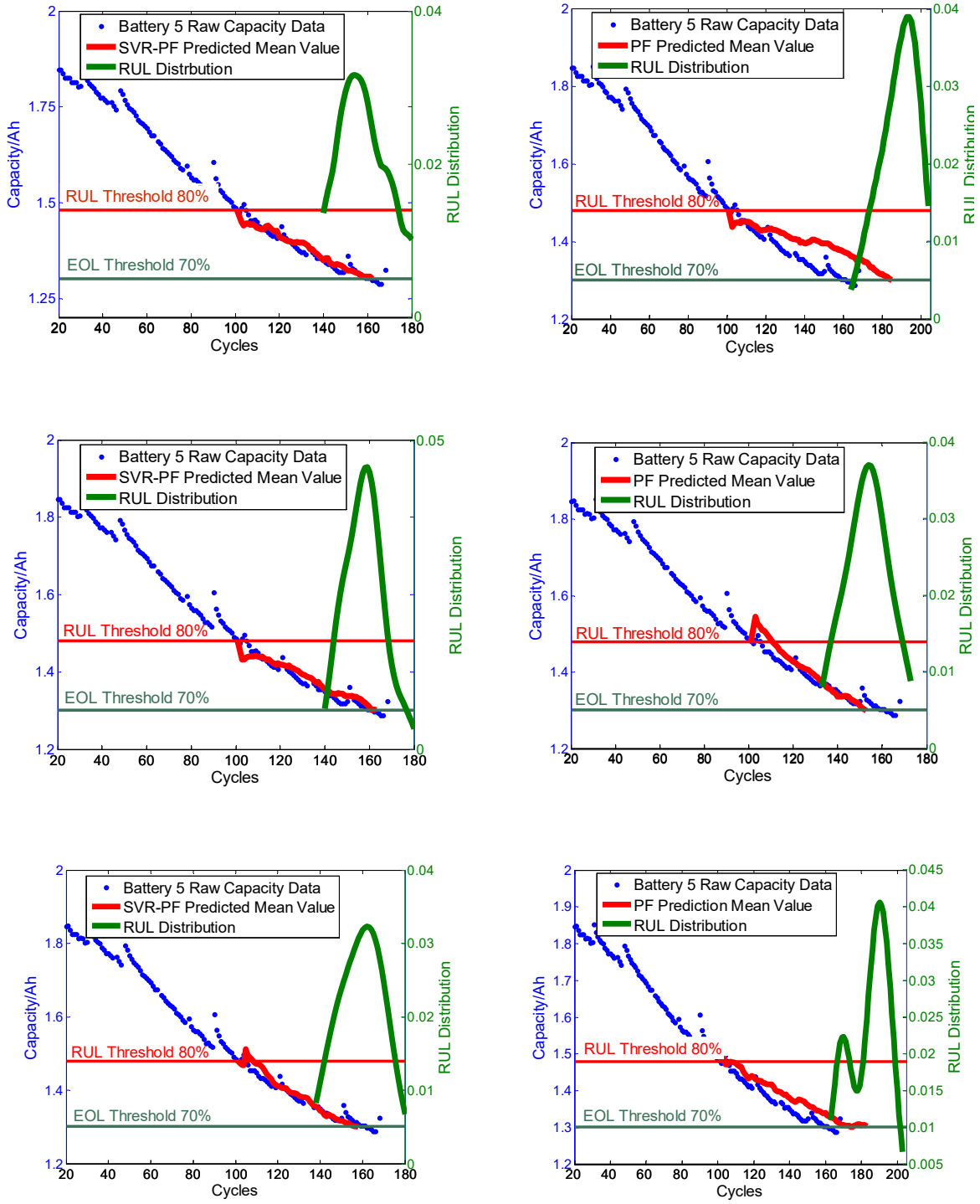

Figure 4-7 SVR-PF and PF predicted capacity and RUL distribution of battery 5

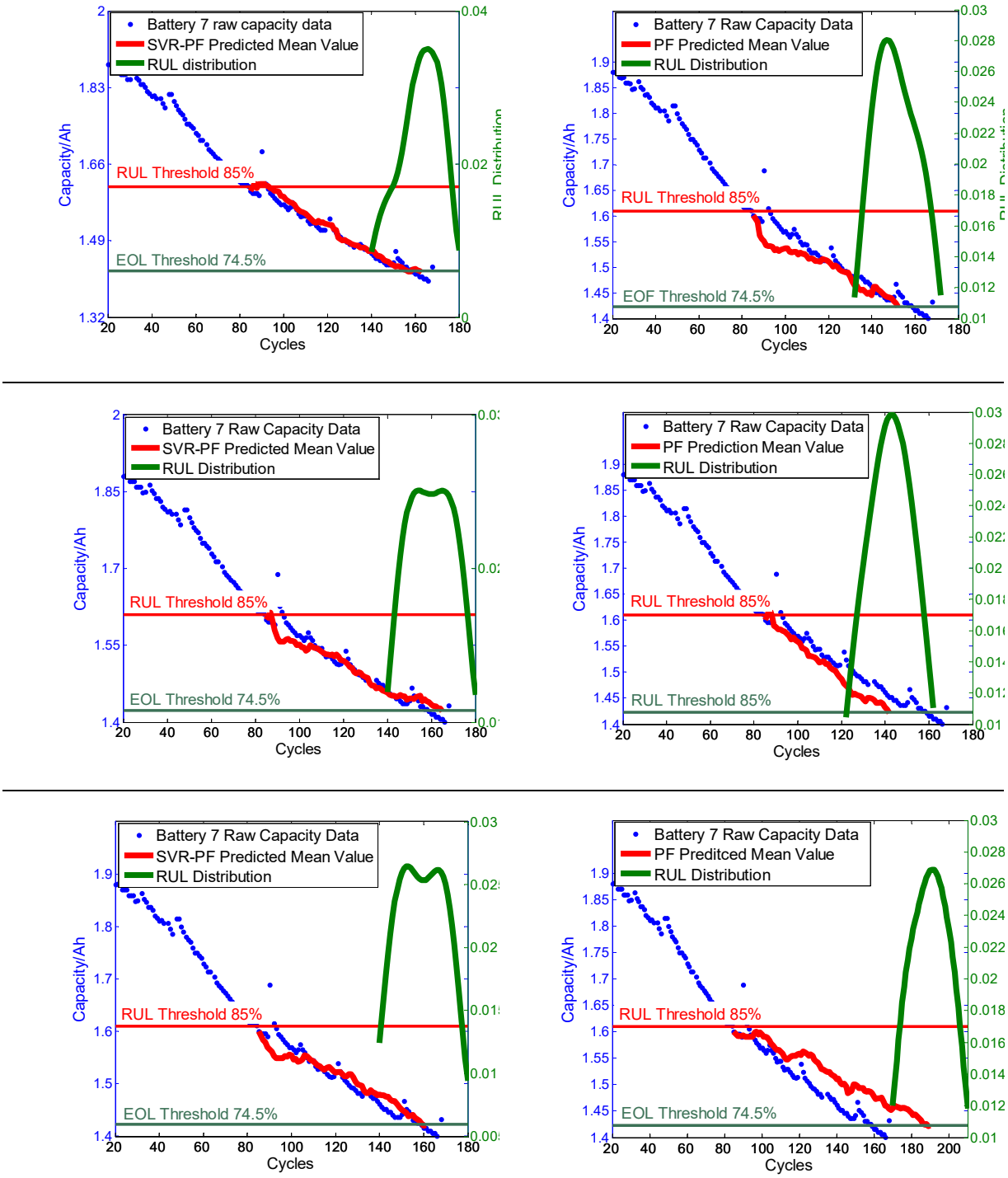

Figure 4-8 SVR-PF and PF predicted capacity and RUL distribution of battery 7

Table **4-2** shows the predicted mean value of EOL and RUL of the algorithm SVR-PF and PF.

Table 4-2 Predicted Mean Value of RUL/EOL (Unit: Cycle)

Simulation Label	Battery 5				Battery 7			
	SVR-PF		PF		SVR-PF		PF	
	RUL	EOL	RUL	EOL	RUL	EOL	RUL	EOL
1	60	161	83	184	78	163	67	152
2	62	163	52	153	80	165	71	142
3	57	158	82	183	76	161	105	190
Measured Value	RUL: 61 EOL: 162				RUL: 75 EOL: 160			

The results show that the SVR-PF algorithm has robust performance when using random initial particles and random samples on posterior distributions.

4.6.3 Effects of RUL Threshold Value on Prediction

To study the effects of RUL threshold value on the prediction performance, we change the RUL threshold value to 85% of nominal capacity for battery 5 and 90% for battery 7. The prediction results for SVR-PF and PF are shown in

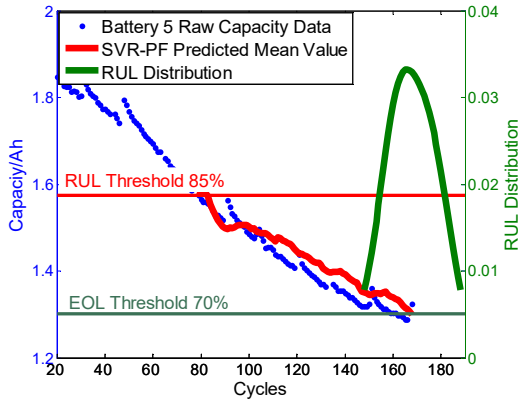

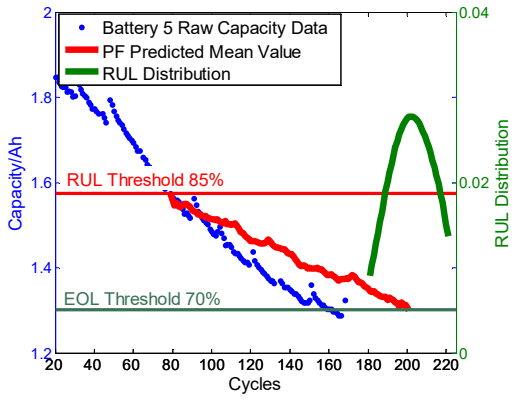

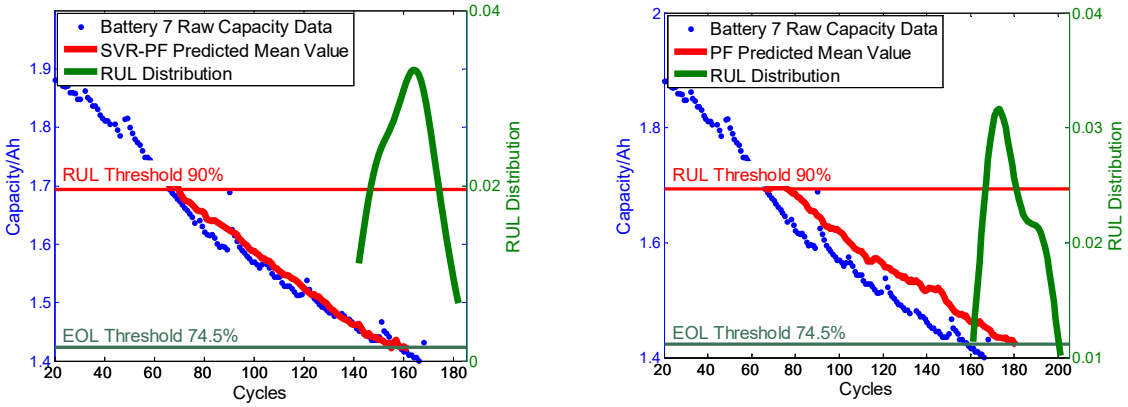

Figure 4-9. The predicted RUL and EOL mean values are shown in Table 4-3.

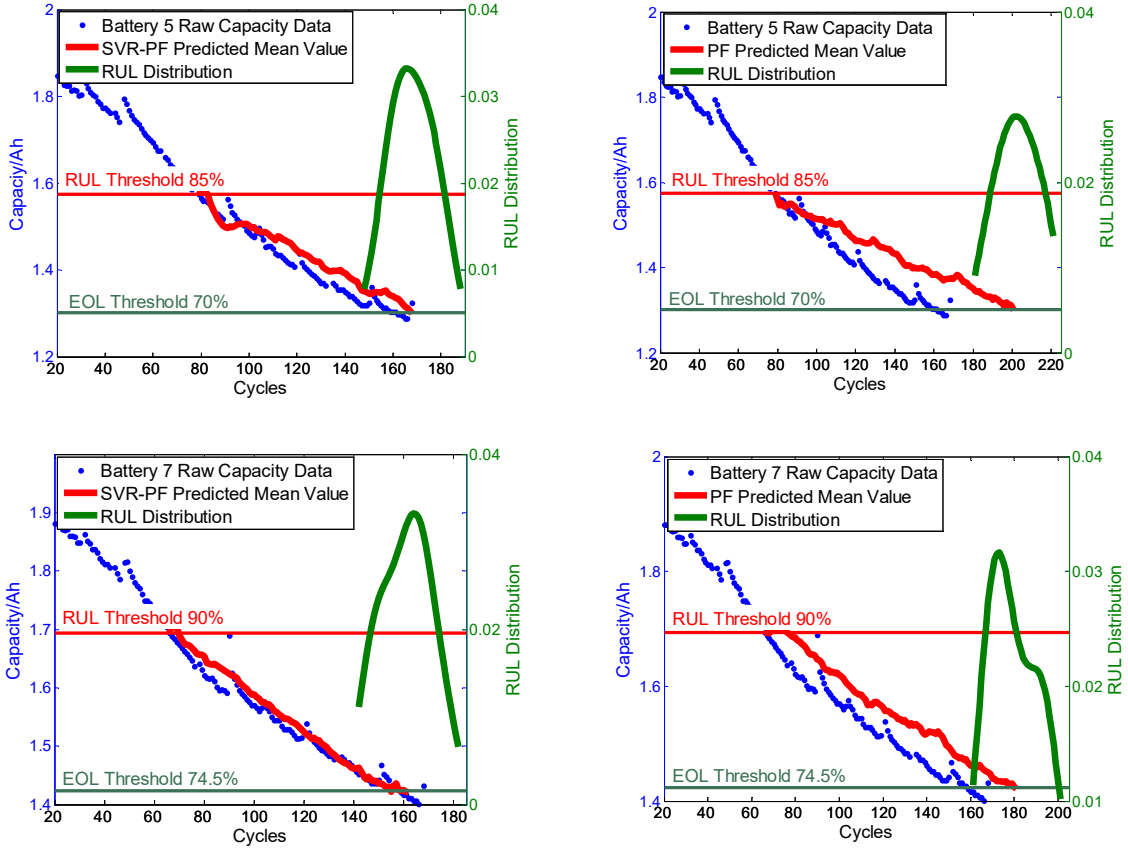

Figure 4-9 Predicted battery RUL distribution at different RUL thresholds

Table 4-3 Predicted RUL/EOL value at different RUL thresholds (Unit: Cycle)

	Battery 5		**Battery 7**	
	RUL	EOL	RUL	EOL
SVR-PF	89	168	96	162
PF	122	201	115	181
Measured Value	83	162	94	160

The prediction results of the proposed SVR-PF method are more accurate than that of the PF method. Moreover, the performance of the PF method deteriorates more quickly than the SVR-PF method as the given data points become fewer. Therefore, the SVR-PF algorithm can provide more robust and accurate prediction of battery RUL.

4.7 Conclusion

In this chapter, we explore an improved method for battery SOH monitoring and RUL prediction. We derive a battery degradation model based on the results of (Goebel, 2009). The main contributions of this research can be summarized as: (1) an accurate model for battery SOH monitoring is developed, which provides a good foundation for multi-step ahead prediction. (2) Battery degradation parameters are extracted to provide accurate RUL prediction together with the aging parameter. (3) The RUL probability distribution is updated over time by a new RUL prediction approach. (4) The battery capacity depletion is analyzed using the novel SVR-PF algorithm. With the experimental data we validate the robustness of the SVR-PF algorithm for battery RUL prognostics and compare its predictive capability to the standard PF algorithm.

Comparing to the research done by Goebel, (Goebel, 2009) and Orchard, (Orchard, 2013), SVR-PF method overcomes the degeneracy phenomenon. The SVR-PF shows improved estimation and prediction capability compared to the standard PF.

CHAPTER 5

Conclusions and Future Work

5.1 Conclusions

This dissertation conducts systematic research on the power batteries' SOH and RUL. The major achievements of this dissertation include combining physics-based model and data-driven model for the estimation of SOH and RUL of a battery even if the battery has unknown degradation properties, and (2) improving the RUL prediction result even the system and noise have non-linear characteristics.

In chapter 2, we have investigated NiH_2 battery performance to develop fault detection, reduce online false alarm rate, and predict the degradation process. ARMA and a hybrid model have been used to establish the data-driven model. The hybrid model provides more accurate one-step ahead prediction results compared with traditional ARMA models. Results from both voltage and pressure measurements show reduced false alarm rate with 95% confidence interval. A multi-step ahead prediction method is also developed for long-term degradation analysis of the NiH_2 battery, by focusing on the pressure growth. The prediction results show the robustness and accuracy of the proposed model by comparing to the test data. In addition, further pressure behavior is predicted to provide health management support information.

In Chapter 3, a method is also preposed for estimating both the state of charge and cell parameters of a Li-ion battery cell over its lifetime using the Dual Extended Kalman Filters. To

determine the state of charge accurately, the electrochemical model is developed to represent the cell dynamics, which is more advanced than equivalent circuit model. The experimental and simulation results show an efficient estimation and quick convergence of the SOC and robust estimation of parameters changing in the long run. The experimental and estimation results show that the discharging capacity and film resistance determined based on the DEKF is valid and effectively represent the degradation process. It can also be inferred that if there is noise in the sensor measurement and battery system itself, the estimations based on the DEKF will be more accurate than that based on the Coulomb counting method due to the noise filtering capability and long-term parameter tuning function.

In chapter 4, an improved method for battery SOH monitoring and RUL prediction is explored. We derive a battery degradation model based on the results of (Goebel, 2009). The main contributions of this research can be summarized as: (1) an accurate model for battery SOH monitoring is developed, which provides a good foundation for multi-step ahead prediction. (2) Battery degradation parameters are extracted to provide accurate RUL prediction together with the aging parameter. (3) The RUL probability distribution is updated over time by a new RUL prediction approach. (4) The battery capacity depletion is analyzed using the novel SVR-PF algorithm. With the experimental data we validate the robustness of the SVR-PF algorithm for battery RUL prognostics and compare its predictive capability to the standard PF algorithm.

5.2 Scientific Contribution

The scientific contributions of the research are summarized as follows:

1. Study the data-driven methods ARMA and ANN for battery RUL prediction when the battery properties and usage environment are relatively stable.

2. Monitor battery SOC and long-term cell parameters of the battery by integrating a simplified electrochemical battery model and Dual Extended Kalman Filter technique.
3. Develop predictive methodology Support Vector Regression-Particle Filter (SVR-PF) algorithm to improve the accuracy and robustness of RUL prediction while facing system nonlinearity and noise nonlinearity.

5.3 Future Work

The future work may include the use of new methodologies such as Unscented Kalman Filter and Particle Filter (UPF) for more accurate battery prognosis. The Extended Kalman Filter (EKF) has been used as the standard technique for performing recursive nonlinear estimation. The EKF algorithm, however, provides only an approximation to optimal nonlinear estimation. We point out the underlying assumptions and flaws in the EKF and present an alternative filter with performance superior to that of the EKF. This algorithm, referred to as the Unscented Kalman Filter (UKF), was first proposed by Julier et al., (Julier, 1995) and further developed by Wan and van der Merwe (Wan, 2000). The basic difference between the EKF and UKF stems from the way Gaussian random variables (GRV) are represented for propagating through system dynamics.

Julier and Uhlman demonstrated the substantial performance gains of the UKF in the context of state estimation for nonlinear control. Several theoretical results were also derived (Julier, 1997). They reviews this work and presents extensions to a broader class of nonlinear estimation problems, including nonlinear system identification, training of neural networks, and dual estimation problems. Additional methedology includes the development of an Unscented Kalman Smoother (UKS), the specification of efficient recursive square-root implementations, and a novel use of the UKF to improve particle filters.

Besides, the particle filter is a sequential Monte Carlo method that allows for a complete representation of the state distribution using sequential importance sampling and resampling. Whereas the standard EKF and UKF make a Gaussian assumption to simplify the optimal recursive Bayesian estimation, particle filters make no assumptions on the form of the probability densities in question; that is, they employ full nonlinear, non-Gaussian estimation. A method that utilizes the UKF to augment and improve the standard particle filter, specifically through the generation of the importance proposal distribution can be considered.

BIBLIOGRAPHY

Akaike, H., 1974. “A new look at the statistical model identification”. IEEE Transactions on Automatic Control 19 (6): 716–723, doi:10.1109/TAC.1974.1100705, MR 0423716

Armand, M., and Tarascon, J., 2008, “Building better batteries,” Nature, Vol. 451, No. 7179, pp. 652-7.

Baltersee, J., Chambers, J.A., 1998. “Nonlinear adaptive prediction of speech with a pipelined recurrent neural network”. IEEE Transactions on Signal Processing, v 46, n 8, p 2207-16.

Bharath P, Krishna P, John P C, et al. “Automotive battery management systems”, CI, IEEE Autotestcon, 2008: 581-586.

Box, P., Jenkins, G. M., 1976. “Time series analysis: Forecasting and control.” San Francisco, CA: Holden-day Inc.

Chaturvedi, N. A., Klein, R,., Christensen, J., Ahmed, J., and Kojic, A., 2010, “Algorithms for advanced battery-management systems,” IEEE Control Systems Magazine, Vol. 30, No. 3, pp. 49-68.

Chen M, Rincon M, Gabriel A. “A compact electrical model formicroscale fuel cells capable of predicting runtime and I-V polarization performance”. IEEE Trans. Power Electron, 2008, 23(3): 842-850.

Cheng, K., Divakar, B.P., Wu, H., Ding, K., and Ho, H., 2011, “Battery-management system (BMS) and SOC development for electrical vehicles,” IEEE Transactions on Vehicular Technology, Vol. 60, No. 1, pp. 76-88.

Corey T L, Maheboob B V, Richard E R, et al. “State-of-healthmonitoring of 18650 4S packs with a single-point impedancediagnostic”. Journal of Power Sources, 2014, 266: 512-519.

Dalton, P., Cohen, F., 2003. “Update on international space station nickel hydrogen battery on-orbit performance”. Proceedings of AIAA, Paper #12066, 2003.

Dalton, P., Cohen, F., 2004 “International space station nickel-hydrogen battery on-orbit performance”, 37th Intersociety Energy Conversion Engineering Conference (IECEC) (IEEE Cat. No.02CH37298), p 106-13.

Danilov, D., Niessen, R.A.H., and Notten, P.H.L., 2011, “Modeling all-solid-state Li-ion batteries,” Journal of the Electrochemical Society, Vol. 158, No. 3, pp A215-A222.

Domenico, D. D, Fiengo, G., and Stefanopoulou, A., 2008, "Lithium-ion Battery state of charge estimation with a Kalman filter based on a electrochemical model," Proceedings of the IEEE International Conference on Control Applications, pp. 702-707.

Domenico, D. D., Stefanopoulou, A., and Fiengo, G., 2010, "Lithium-Ion Battery State of Charge and Critical Surface Charge Estimation Using an Electrochemical Model-Based Extended Kalman Filter," Journal of Dynamic Systems, Measurement and Control, Vol. 132, No. 6, pp. 061302.

Doyle, M., and Fuentes, Y., 2003, "Computer simulations of a lithium-ion polymer battery and implications for higher capacity next-generation battery designs," Journal of Electrochemistry Society, Vol. 150, pp. A706–A713.

Dubarry, M., Vuillaume, N., and Liaw, B., 2010, "Origins and accommodation of cell variations in Li-ion battery pack modeling," International Journal of Energy Research, Vol. 34, No. 2, pp. 216-231.

Farag, M., Ahmed, R., Gadsden, S.A., Habibi, S.R., and Tjong, J., 2012, "A comparative study of Li-ion battery models and nonlinear dual estimation strategies," 2012 IEEE Transportation Electrification Conference and Expo (ITEC), pp. 8.

Ferreira, J. C., Menegatto, V. A., "Eigenvalues of integral operators defined by smooth positive definite kernels", Integral equation and Operator Theory, 64 (2009), no. 1, 61–81

Francisco, J. M., Fox, C. L., Cook, W. D., 1997. "Life cycle testing of spaceflight qualified nickel-hydrogen battery cells", Proceedings of the Thirty-Second Intersociety Energy Conversion Engineering Conference, p 149-53 vol.1.

Goebel, K., Saha, B., Saxena, A., Celaya, J., and Christophersen, J., 2008. "Prognostics in battery health management". IEEE Instrumentation & Measurement Magazine, v 11, n 4, p 33-40

Haykin, S., 1995. "Nonlinear Adaptive Prediction of Nonstationary Signals". IEEE Trans. Signal Processing, Vol. 43, No. 2.

He, H., Xiong, R., Guo, H., and Li, S., 2012, "Comparison study on the battery models used for the energy management of batteries in electric vehicles," Energy Conversion and Management, Vol. 64, 113–121.

He, W., Williard, N., Chen, C., and Pecht, M., 2012, "State of charge estimation for electric vehicle batteries under an adaptive filtering framework," Proceedings of IEEE 2012 Prognostics and System Health Management Conference, PHM-2012.

Hollandsworth, R.P., Armantrout, J.D., and Rao, G.M., 2002. "NiH_2 Reliability Impact Upon Hubble Space Telescope Battery Replacement". 37th lntersociety Energy Conversion Engineering Conference (IECEC) Page(s): 276 – 281

Hu Xs, Li S B, Peng H. "A comparative study of equivalent circuit models forLi-ion batteries". Journal of Power Sources, 2012, 198: 359-367

Hu, C., Youn, B., and Chung, J., 2012, "A multiscale framework with extended Kalman filter for lithium-ion battery SOC and capacity estimation," Applied Energy, Vol. 92, pp. 694-704.

Iwakura, C., Kajiya, Y., Yoneyama, H., Saki, T., Oguro, K., Ishikawa, H., 1989. "Self-discharge mechanism of nickel-hydrogen batteries using metal hydride anodes", Journal of the Electrochemical Society, v 136, n 5, p 1351-1355

Jardine Ak S, Lin D, Banjevic D. "A review on machinery diagnosticsand prognostics implementing condition based maintenance". Mechanicasystems and signal processing in press, 2006, 20(7): 1483-1510.

Johnson V H. "Battery performance models in ADVISOR", Journal ofPower Sources. 2002, 110(2): 321-329.

Julier S., Uhlmann J., Durrant-Whyte H., "A new approach for filtering nonlinear systems", Computer Science, Proceedings of 1995 American Control Conference - ACC'95, 1995

Julier S., Uhlmann J., "New extension of the Kalman filter to nonlinear systems", Computer Science, Engineering,Defense, Security, and Sensing, 1997

Khashei, M., Zeinal H., A., Bijari, M., 2012. "A novel hybrid classification model of artificial neural networks and multiple linear regression models". Expert Systems with Applications, v 39, n 3, p 2606-2620.

Kroeze R C, Krein P T. "Electrical battery model for use in dvnamic electricvehicle simulations". IEEE Power Electronics Specialists Conference, 20081336-1342

Li F, Xu J P. "A new prognostics method for state of health estimation oflithium-ion batteries based on a mixture of Gaussian process models and particle filter". Microelectronics Reliability, 2015, 55(7): 1035-1045

Liaw B Y, Ganesan N, Jungst R G, et al. "Modeling of lithium ion cells- A simple equivalent-circuit model approach". Solid State lonics, 2004,175(1-4): 835-839.

Lu L G, Han Xb, Li Jq, et al. "A review on the key issues for li-ion batterymanagement in electric vehicles". Joumnal of Power Sources, 2013, 226:272-288.

Meissner E, Richter G. “Battery Monitoring and Electrical EnergyManagement Pre condition for future Vehicle electric power systems”. Joumal of Power Sources, 2003, 116: 79-98

Meissner E, Richter G. “The challenge to the automotive battery industrythe battery has to becomean increasingly integrated component”. Joumal ofPower Sources, 2005 , 144: 438-460

Mohamad H. Hassoun, 1995, “Fundamentals of Artificial Neural Networks”, Cambridge, MA: MIT Press, 1995

Mohammad C. Mohammad F. “State-of-charge estimation for lithium-ionbatteries using neural networks and EKF”. IEEE Transactions on IndustrialElectronics, 2010, 57(12): 4178-4187.

Moura, S.J., Forman, J.C., Bashash, S., Stein, J. L., and Fathy, H. K., 2011, “Optimal control of film growth in lithium-ion battery packs via relay switches,” IEEE Transactions on Industrial Electronics, Vol. 58, No. 8, pp. 3555-3566.

Ning, G., and Popov, B. N., 2004, “Cycle Life Modeling of Lithium-Ion Batteries,” Journal of The Electrochemical Society, Vol. 151, No. 10, pp. A1584-A1591.

Ondrej L, Edward Jw, Matthew H, et al. “Intelligent neural network implementation for SOCI development of Li/CFx batteries”. 2009-2nd International Symposium on Resilient Control Systems, 2009: 57-62

Plett, G.L., 2004, “Extended Kalman filtering for battery management systems of LiPB-based HEV battery packs. Part 1. Background,” Journal of Power Sources, Vol. 134, No. 2, pp. 252-61.

Plett, G.L., 2004, “Extended Kalman filtering for battery management systems of LiPB-based HEV battery packs. Part 3. State and parameter estimation,” Journal of Power Sources, Vol. 134, No. 2, pp. 277-92.

Purushothaman, B.K., Wainright, J.S., 2012. “Analysis of pressure variations in a low-pressure nickel-hydrogen battery: Part 1”. Journal of Power Sources, v 206, p 429-35

Remmlinger J, Buchholz M, Meiler M, Bernreuter P, Dietmayer K. “State-of-health monitoring of lithium-ion batteries in electric vehicles by on-board internal resistance estimation”. Joural of Power Sources,2011, 196(12): 5325-5331

Rezvanizaniani S M, Liu Z, Chen Y, Lee J, “Review and recent advances in battery health monitoring and prognostics technologies for electric vehicle (EV) safety and mobility”, Journal of Power Sources15 June 2014Volume 256Pages 110-124

Samadani, S., Fraser, R., and Fowler, M., 2012, “A Review Study of Methods for Lithium-ion Battery Health Monitoring and Remaining Life Estimation in Hybrid Electric Vehicles,” SAE Technical Paper, 2012-01-0125, doi:10.4271/2012-01-0125.

Santhanagopalan, S., and White, R. E., 2006, “Online Estimation of the State of Charge of a Lithium Ion Cell,” Journal of Power Sources, Vol. 161, pp. 1346–1355.

Sarre, G., Blanchard, P., and Broussely, M., 2004, “Aging of lithium-ion batteries,” Journal of Power Sources, Vol. 127, No. 1-2, pp. 65-71.

Sikha, G., White, R., and Popov, B., 2005, “A mathematical model for a lithium-ion battery/electrochemical capacitor hybrid system,” Journal of the Electrochemical Society, Vol. 152, No. 8, pp. A1682-A1693.

Smith, K. A., Rahn, C. D., and Wang, C., 2010, “Model-Based Electrochemical Estimation and Constraint Management for Pulse Operation of Lithium Ion Batteries,” IEEE Transactions on Control Systems Technology, Vol. 18, No. 3.

Smithrick, J., O'Donnell, P. M., 1996. “Nickel hydrogen batteries - An overview”. J. of Propulsion and Power, Vol. 12, No. 5, pp. 873-878.

Song B, Li E W. “Study on state of health for power transformer oil withmultiple parameters”. 2014 International Conference on Power SystemTechnology: Towards Green, Efficient and Smart Power System, 2014:462-1466.

Subhadeep B, Pavol B. “Online state-of-charge estimation of a liFePo4battery for real electric vehicle driving scenario and modeling of the batteryparameters for different driving conditions”. 2012 International Exhibitionand Conference for Power Electronics, Intelligent Motion, Renewable Energyand Energy Management, 2012: 1493-1500.

Turevs. Murat C, Abdulkadir B. “An analytical battery state of healthestimation method”. IEEE Intemational Svmposiun on Industrial Electronics.2014: 1605-1609

Vidts, P. D., Delgado, J., and White, R.E., 1995, “Mathematical modeling for the discharge of a metal hydride electrode,” Journal of the Electrochemical Society, Vol. 142, No. 12, pp. 4006-13.

Wan E., R. Merwe V., “The unscented Kalman filter for nonlinear estimation”, Proceedings of the IEEE Adaptive Systems for Signal Processing, Communications, and Control Symposium (Cat. No.00EX373), 2000

Wang J, Wang H P, Lu Fg, et al. “Analysis of Al-steel resistance spotwelding process by developing a fully coupled multi-physics simulationmodel”. 2015, 89: 1061-1072.

Xing Y J, Eden W M M, Kwok Lt, et al. “Battery Management Systems in Electric and Hybrid Vehicles”. Energies, 2011, 4: 1840-1857.

Zhang, J., and Lee, J., 2011. “A review on prognostics and health monitoring of Li-ion battery”, Journal of Power Sources, Vol. 196, No. 15, pp. 6007-6014.

Zimmerman, A. H., 2008. “Nickel-hydrogen batteries: principles and practice”. The Aerospace Press, ISBN 1-884989-20-9

Zou Y, Hu Xs, Ma H M, et al. “Combined State of Charge and State of Health estimation over lithium-ion battery cel cycle life span for electricvehicles”. Journal of Power Sources, 2015, 273: 793-803.